

Monte Carlo study of an improved clock model in three dimensions

Martin Hasenbusch*

*Institut für Theoretische Physik, Universität Heidelberg,
Philosophenweg 19, 69120 Heidelberg, Germany*

(Dated: March 18, 2022)

Abstract

We study a generalized clock model on the simple cubic lattice. The parameter of the model can be tuned such that the amplitude of the leading correction to scaling vanishes. In the main part of the study we simulate the model with Z_8 symmetry. At the transition, with increasing length scale, $O(2)$ symmetry emerges. We perform Monte Carlo simulations using a hybrid of local Metropolis and cluster algorithms of lattices with a linear size up to $L = 512$. The field variable requires less memory and the updates are faster than for a model with $O(2)$ symmetry at the microscopic level. Our finite size scaling analysis yields accurate estimates for the critical exponents of the three-dimensional XY-universality class. In particular we get $\eta = 0.03810(8)$, $\nu = 0.67169(7)$, and $\omega = 0.789(4)$. Furthermore we obtain estimates for fixed point values of phenomenological couplings and critical temperatures.

* M.Hasenbusch@thphys.uni-heidelberg.de

I. INTRODUCTION

In the neighborhood of a second order phase transition, thermodynamic quantities diverge, following power laws. For example the correlation length ξ behaves as

$$\xi = a_{\pm}|t|^{-\nu} (1 + b_{\pm}|t|^{\theta} + ct + \dots) , \quad (1)$$

where $t = (T - T_c)/T_c$ is the reduced temperature. The subscript \pm of the amplitudes a_{\pm} and b_{\pm} indicates the high (+) and the low (-) temperature phase, respectively. Second order phase transitions are grouped into universality classes. For all transitions within such a class, critical exponents like ν assume the identical value. These power laws are affected by corrections. There are non-analytic or confluent and analytic ones. The leading corrections are explicitly given in eq. (1). Also correction exponents such as $\theta = \omega\nu$ are universal. For the system discussed here, $\theta \approx 0.5$. Amplitudes such as a_{\pm} and b_{\pm} depend on the microscopic details of the system. However certain combinations, so called amplitude ratios, assume universal values. Universality classes are characterized by the symmetry properties of the order parameter at criticality, the range of the interaction and the spacial dimension of the system. For reviews on critical phenomena see for example [1–4].

Note that in general the symmetry properties of the order parameter can not be naively inferred from the microscopic properties of the system. In particular a symmetry might emerge that is not present in the classical Hamiltonian. For example, in the model studied here, the symmetry is enhanced from Z_N to $O(2)$ at the critical point. At the $O(2)$ -invariant Wilson-Fisher fixed point in three dimensions, a perturbation that breaks the $O(2)$ -invariance down to Z_N -invariance is irrelevant in the sense of the renormalization group (RG) for $N \geq 4$. See ref. [5] and references therein. Monte Carlo studies have shown that the transition of N -state clock models on the simple cubic lattice are in the domain of attraction of the $O(2)$ -invariant fixed point for $N \geq 5$. See for example ref. [6]. The major part of our simulations are performed for $N = 8$. The related RG-exponent takes the value $y_{N=8} = -5.278(9)$, see table II of ref. [5]. Therefore, the deviations from $O(2)$ -invariance rapidly vanish with increasing lattice size and can be safely ignored in the finite size scaling analysis at the critical point. The Z_N -invariant perturbation is dangerously irrelevant. In the low temperature phase, in the thermodynamic limit, the spontaneous magnetization might only assume one of the N directions, that are preferred by the Hamiltonian. See for example ref. [7] and references therein. In the present work, we focus on the critical point and consider a

model with Z_N -symmetry mainly for technical reasons. Less memory is needed to store the configurations and the updates require less CPU-time than for a model with $O(2)$ symmetry.

The three-dimensional XY-universality class has attracted much attention, since the λ -transition of ^4He , which is well studied experimentally, is supposed to share this universality class. The most accurate result for the exponent α of the specific heat is obtained from an experiment under the condition of microgravity [8–10]:

$$\alpha = -0.0127(3) \quad , \quad (2)$$

which corresponds to $\nu = (2 - \alpha)/d = 0.6709(1)$.

The three-dimensional XY-universality class has been studied by using various theoretical approaches. For example field theoretic methods, high and low temperature series expansions and Monte Carlo simulations of lattice models. A few representative results for critical exponents are given in table I. Note that other critical exponents can be obtained from ν and η by using scaling relations. For more comprehensive collections see table I of ref. [16], table 19 of ref. [4], or table I of ref. [13]. Recently great progress has been achieved by using the so called conformal bootstrap method. In particular in the case of the three-dimensional Ising universality class, the accuracy that has been reached for critical exponents clearly surpasses that of other theoretical methods. See ref. [17] and references therein. For the XY and the $O(3)$ universality classes in three dimensions the results obtained so far, are less precise. The estimates given in table I are derived from the numbers for the scaling dimensions Δ_ϕ and Δ_s given in ref. [14]. Note that after we had put the first version of this paper on arXiv, ref. [15] has been submitted. The accurate results, that come with rigorous bounds, are in nice agreement with ours. In the last row of table I we report as preview the results of the present work. We fully confirm ref. [12], the discrepancy with the experiment [8–10] remains.

An important feature of refs. [12, 16] is that so called improved models are studied. One considers models that have one parameter in addition to the inverse temperature and the external field. On the critical line, the amplitude b_\pm of leading corrections to scaling, eq. (1), depends on this parameter. If there exists a value of the parameter with $b_\pm = 0$, RG-theory predicts that the same holds for all quantities that are singular at the transition. In the following we shall call a model with $b_\pm = 0$ an improved model. The idea had been exploited first by using high temperature series expansions of such models [18, 19]. For early Monte

TABLE I. A few representative results for the critical exponents ν , η and ω for the universality class of the three-dimensional XY model obtained by various theoretical methods. MC+HT means that Monte Carlo simulations and the analysis of high temperature expansions have been combined to analyze the lattice models under consideration.

Ref.	method	year	ν	η	ω
[11]	ϵ -expansion	1998	0.6680(35)	0.0380(50)	0.802(18)
[11]	3D-expansion	1998	0.6703(15)	0.0354(25)	0.789(11)
[12]	MC+HT	2006	0.6717(1)	0.0381(2)	0.785(20)
[13]	MC	2019	0.67183(18)	0.03853(48)	0.77(13)
[14]	conformal bootstrap	2016	0.6719(11)	0.03852(64)	
[15]	conformal bootstrap	2019	0.67175(10)	0.038176(44)	
present work	MC	2019	0.67169(7)	0.03810(8)	0.789(4)

Carlo simulations of improved models sharing the universality class of the three-dimensional Ising model see for example refs. [20–22].

In the present work, we study a generalization of the N -state clock model, which is closely related with the ddXY model that has been studied in refs. [12, 16]. In addition to the N values on the unit circle, the field variable might take the value $(0, 0)$ in the center of the circle. We refer to this model as $(N + 1)$ -state clock model. Its precise definition is given in section II below.

We study the model by using finite size scaling (FSS) [23]. The outline of the study builds upon our previous work on critical phenomena, see for example refs. [12, 16, 22, 24–27], to give only a few. An important feature of these studies is that in addition to the Binder cumulant [28], other dimensionless ratios like the second moment correlation length over the linear lattice size ξ_{2nd}/L or the ratio of the partition functions for periodic and anti-periodic boundary conditions Z_a/Z_p are exploited. The comparison of results obtained from these different quantities allows us to estimate systematical errors that are caused by subleading corrections that are not explicitly taken into account in the fits.

The purpose of the present work is twofold. First we improve the accuracy of the critical exponents of the three-dimensional XY universality class. These results provide a benchmark

for future theoretical progress achieved by the conformal bootstrap or other methods. In fact, in the case of ref. [15] this already occurred. Second we provide non-universal results, like for example inverse critical temperatures, which are important groundwork for future studies. In particular we intend to compute the structure constants using a similar approach as in ref. [29] for the Ising universality class. Furthermore the improved $(N + 1)$ -state clock model should be a good starting point to study the symmetry properties of the order parameter in the low temperature phase.

The outline of the manuscript is the following: In section II we define the model and the observables that we measured. We summarize the theoretical basis of our finite size scaling analysis in section III. In section IV we discuss the Monte Carlo algorithm used in the simulations. In section V we analyze the data and present the results for the fixed point values of the dimensionless ratios, inverse critical temperatures, the correction exponent ω , and the critical exponents ν and η . Finally we conclude and give an outlook. In the appendix we discuss the dependence of the critical temperature and other non-universal quantities on N and determine the RG-exponent $y_{N=6}$ related to a Z_6 invariant perturbation of the $O(2)$ invariant fixed point.

II. THE $(N + 1)$ -STATE CLOCK MODEL

The model can be viewed as a generalization of the N -state clock model. The field \vec{s}_x at the site $x = (x_0, x_1, x_2)$, where $x_i \in 0, 1, 2, \dots, L_i - 1$, might assume one of the following values

$$\vec{s}_x \in \{(0, 0), (\cos(2\pi m/N), \sin(2\pi m/N))\} , \quad (3)$$

where $m \in \{1, \dots, N\}$. Compared with the N -state clock model, $(0, 0)$ is added as possible value of the field variable. In our program, we store the field variables by using labels $m = 0, 1, 2, \dots, N$. We assign

$$\vec{s}(0) = (0, 0) \quad (4)$$

and for $m > 0$

$$\vec{s}(m) = (\cos(2\pi m/N), \sin(2\pi m/N)) . \quad (5)$$

The reduced Hamiltonian is given by

$$\mathcal{H} = -\beta \sum_{\langle xy \rangle} \vec{s}_x \cdot \vec{s}_y - D \sum_x \vec{s}_x^2 - \vec{H} \sum_x \vec{s}_x , \quad (6)$$

where $\langle xy \rangle$ denotes a pair of nearest neighbor sites on the simple cubic lattice. We introduce the weight factor

$$w(\vec{s}_x) = \delta_{0,\vec{s}_x^2} + \frac{1}{N} \delta_{1,\vec{s}_x^2} = \delta_{0,m_x} + \frac{1}{N} \sum_{n=1}^N \delta_{n,m_x} \quad (7)$$

that gives equal weight to $(0,0)$ and the collection of all values $|\vec{s}_x| = 1$. Now the partition function can be written as

$$Z = \sum_{\{\vec{s}\}} \prod_x w(\vec{s}_x) \exp(-\mathcal{H}) , \quad (8)$$

where $\{\vec{s}\}$ denotes a configuration of the field. Note that in the limit $N \rightarrow \infty$, we recover the dynamically diluted XY (ddXY) model studied in refs. [12, 16]. The reduced Hamiltonian of the ddXY model has the same form as eq. (6):

$$\mathcal{H}_{ddXY} = -\beta \sum_{\langle xy \rangle} \vec{\phi}_x \cdot \vec{\phi}_y - D \sum_x \vec{\phi}_x^2 - \vec{H} \sum_x \vec{\phi}_x , \quad (9)$$

where $\vec{\phi}_x$ is a vector with two real components. The partition function is given by

$$Z = \prod_x \left[\int d\mu(\phi_x) \right] \exp(-\mathcal{H}_{ddXY}) , \quad (10)$$

with the local measure

$$d\mu(\phi_x) = d\phi_x^{(1)} d\phi_x^{(2)} \left[\delta(\phi_x^{(1)}) \delta(\phi_x^{(2)}) + \frac{1}{2\pi} \delta(1 - |\vec{\phi}_x|) \right] . \quad (11)$$

Note that the dynamically diluted XY model is a special case ($K = 0$) of the vectorialized Blume, Emery, and Griffiths (VBEG) model studied in ref. [30].

A. Phase diagram of the dynamically diluted XY model

We expect that the phase diagram for $N \geq 5$ is essentially the same as that of the ddXY model. Therefore we briefly recall the results obtained in refs. [12, 16]. In the limit $D \rightarrow \infty$ the XY model is recovered. There is a line of second order phase transitions that ends at D_{tri} in a tricritical point. Following ref. [16], based on mean-field calculations, $D_{tri} < 0$. Along the line of second order phase transitions, there is a D^* , where leading corrections to scaling vanish. We refer to the ddXY model at $D \approx D^* = 1.06(2)$, ref. [12], as improved ddXY model. In table II we summarize results obtained for the inverse critical temperature β_c at various values of D . In the Appendix B we shall study the N -dependence of β_c in detail.

TABLE II. Results for the inverse of the critical temperature β_c for the dynamically diluted XY model. These results are taken from table II of ref. [12].

D	β_c
0.9	0.5764582(15)[9]
1.02	0.5637963(2)[2]
1.03	0.5627975(7)[7]
1.2	0.5470376(17)[6]
∞	0.4541652(5)[6]

B. Definitions of the measured quantities

The quantities studied are essentially the same as in [12]. For completeness we list them below: The energy density is defined as

$$E = \frac{1}{V} \sum_{\langle xy \rangle} \vec{s}_x \cdot \vec{s}_y. \quad (12)$$

The magnetic susceptibility χ for a vanishing magnetization and the second moment correlation length ξ_{2nd} are defined as

$$\chi = \frac{1}{V} \left\langle \left(\sum_x \vec{s}_x \right)^2 \right\rangle \quad (13)$$

and

$$\xi_{2nd} = \sqrt{\frac{\chi/F - 1}{4 \sin^2 \pi/L}}, \quad (14)$$

where

$$F = \frac{1}{V} \left\langle \left| \sum_x \exp\left(i \frac{2\pi x_1}{L}\right) \vec{s}_x \right|^2 \right\rangle \quad (15)$$

is the Fourier transform of the correlation function at the lowest non-zero momentum. We consider several dimensionless quantities, which are also called phenomenological couplings. These quantities are, in the critical limit, invariant under RG transformations. We consider the Binder cumulant U_4 and its sixth-order generalization U_6 , defined as

$$U_{2j} = \frac{\langle (\vec{m}^2)^j \rangle}{\langle \vec{m}^2 \rangle^j}, \quad (16)$$

where $\vec{m} = \frac{1}{V} \sum_x \vec{s}_x$ is the magnetization of the system. We also consider the ratio $R_Z = Z_a/Z_p$ of the partition function Z_a of a system with anti-periodic boundary conditions in one of the three directions and the partition function Z_p of a system with periodic boundary conditions in all directions. Anti-periodic boundary conditions in 0-direction are obtained by changing the sign of the term $\vec{s}_x \cdot \vec{s}_y$ of the Hamiltonian for links $\langle xy \rangle$ that connect the boundaries, i.e., for $x = (L, x_1, x_2)$ and $y = (0, x_1, x_2)$. In order to avoid microscopic effects at the boundary, we require that $-\vec{s}_x$ is in the same set of values as \vec{s}_x . Therefore in the main part of the study N is chosen to be even. In the following we will refer to dimensionless ratios by R . Derivatives of dimensionless ratios with respect to the inverse temperature

$$S_R = \frac{\partial R}{\partial \beta} \quad (17)$$

are used to determine the critical exponent ν . In the following these quantities are also denoted by slope of R .

For most of our analysis we need the observables as a function of β in a certain neighborhood of the critical point. To this end, we simulate at β_s , which is a good approximation of β_c . In order to extrapolate in β we compute the coefficients of the Taylor series in $\beta - \beta_s$ for all quantities listed above up to the third order. Note that a reweighting analysis is not possible, since, due to the large statistics, we performed a binning of the data already during the simulation.

III. FINITE SIZE SCALING: THEORETICAL BACKGROUND

The account given below is similar to section II B of ref. [16]. The main purpose is to make the present paper self contained. Our assumptions concerning subleading corrections differ from ref. [16]. See section III A below. Our starting point is the finite size scaling behavior of the reduced free energy density, which is defined by

$$f(\beta, h, D, L) = -\frac{1}{V} \ln Z(\beta, h, D, L) , \quad (18)$$

where Z is the partition function and $V = L^3$ is the number of lattice sites. Note that there is also a dependence on N that we suppress in the following to keep the notation tractable.

The reduced free energy density can be written in terms of the analytic functions \mathcal{F}_{sing} and g , see for example eq. (2.14) of ref. [4],

$$f(\beta, h, D, L) = L^{-d} \mathcal{F}_{sing}(L^{y_t} u_t, L^{y_h} u_h, \{u_i L^{y_i}\}) + g(\beta, h, D) , \quad (19)$$

where d is the dimension of the system. Note that \mathcal{F}_{sing} is a universal function, which however depends on the global geometry of the system, for example on aspect ratios L_i/L_j , where $i \neq j$ are the directions on the lattice or on the type of boundary conditions. Here we consider periodic and anti-periodic boundary conditions that do not generate boundary contributions like Dirichlet boundary conditions for example. The analytic background $g(\beta, h, D)$ does not depend on these global properties. u_t and u_h are the temperature like and external field like scaling fields with the RG-exponents y_t and y_h , respectively. These are the only relevant RG-exponents: $y_t > 0$ and $y_h > 0$. In addition there are irrelevant RG-exponents $y_i < 0$. Below we summarize results on irrelevant RG-exponents given in the literature. Following for example ref. [4], section 1.5.7, the non-linear scaling fields can be written as

$$u_t = g_{01}(D) t + g_{11}(D) t^2 + g_{12}(D) h^2 + O(t^3, th^2, h^4), \quad (20)$$

$$u_h = g_{02}(D) h [1 + g_{12}(D) t + g_{22}(D) h^2 + O(t^2, th^2, h^4)] , \quad (21)$$

where we define the reduced temperature as $t = \beta_c(D) - \beta$. Note that $\beta_c(D)$ and the coefficients $g_{ij}(D)$ depend on N . In appendix B we show however that there is a fast convergence as $N \rightarrow \infty$. The external field is written as $\vec{H} = h\vec{H}_0$, where \vec{H}_0 is a two-component unit vector. We have introduced $g_{01}(D)$ and $g_{02}(D)$ to get the same function \mathcal{F}_{sing} for all values of D on the critical line. The scaling field of the leading correction is

$$u_3 = g_{13}(D) + g_{23}(D) t + g_{33}(D) h^2 + O(t^2, th^2, h^4). \quad (22)$$

The improved model is characterized by $g_{13}(D^*) = 0$. Note that in general $g_{23}(D^*) \neq 0$ and $g_{33}(D^*) \neq 0$. Also note that D^* depends on N , since $g_{13}(D)$ depends on N . For numerical results see appendix B 3.

A. Irrelevant RG-exponents

Let us briefly summarize results on RG-exponents for the three-dimensional XY-universality class given in the literature. Various methods give a, at least qualitatively, consistent picture for the relevant RG-eigenvalues y_t and y_h and the leading irrelevant RG-eigenvalue y_3 . Using scaling relations, see for example ref. [4], sects. 1.3 and 1.5.1, these are related with the critical exponents given in table I as

$$y_t = 1/\nu, \quad y_h = \frac{d+2-\eta}{2}, \quad y_3 = -\omega. \quad (23)$$

Scaling fields can be classified according to the symmetry properties of the operators associated to them. The simple cubic lattice breaks the Galilean symmetries of continuous space. The leading correction associated has the RG-exponent $y_{NR} = -2.02(1)$ [12, 16, 31]. Note that in the case of the three-dimensional Ising universality class, $y_{NR} = -2.0208(12)$ given in table I of ref. [33] is in reasonable agreement with $y_{NR} = -2.022665(28)$ that follows from $\Delta = 5.022665(28)$ for angular momentum $l = 4$ given in table 2 of ref. [17].

Results for subleading corrections are provided by different incarnations of the renormalization group. Newman and Riedel [34] studied the fixed point of the $O(N)$ invariant ϕ^4 theory in three dimensions using the scaling field method. They predict by using the scaling field method subleading corrections with $y_{421} = -1.77(7)$ and $y_{422} = -1.79(7)$, which are nearly degenerate. For the meaning of the indices see ref. [34]. In refs. [12, 16] the analysis of the data is based on this result. Note that Newman and Riedel find $y_{422} = -1.67(11)$ in the case of the Ising universality class, which is not confirmed by the conformal bootstrap method. Instead, $y'' = -3.8956(43)$ is found, see the estimate related to the operator ϵ'' given in table 2 of ref. [17]. In fact, the estimates for subleading correction exponents obtained by the functional renormalization group (FRG), see for example ref. [35], are in better agreement with those of the conformal bootstrap method. In table 3 of ref. [36] results for correction exponents for a large range of N , where N refers to the $O(N)$ symmetry of the theory, are given. The qualitative picture is the same for all N and the numerical values change slowly with varying N . Therefore we regard it as plausible that $-3.5 \gtrsim y'' \gtrsim -4$ for the three-dimensional XY-universality class. Note that skipping corrections $\propto L^{-1.77}$ in the analysis of our data virtually does not change the central values of the final results. Estimates of the error are reduced by a factor of $\approx 2/3$.

Finally let us recall the results for the RG-exponent associated with a Z_N invariant perturbation. The authors of ref. [5] obtain $-y_N = 0.128(6), 1.265(6), 2.509(7), 3.841(8), 5.278(9), 6.796(9), 8.399(10), 10.077(11),$ and $11.825(12)$ for $N = 4, 5, 6, \dots, 12$, respectively. In the main part of our study we have simulated the $(N + 1)$ -state clock model for $N = 8$. For this value of N , we can ignore deviations from $O(2)$ -invariance in the finite size scaling analysis of our data as can be clearly seen from the analysis presented in appendix B4.

B. The magnetic susceptibility and the energy density

The magnetic susceptibility at $h = 0$ for vanishing magnetization is

$$\chi = -\frac{2}{V} \left. \frac{\partial^2 f}{\partial h^2} \right|_{h=0} = \frac{1}{V} \left\langle \left(\sum_x \vec{s}_x \right)^2 \right\rangle. \quad (24)$$

Note that we have introduced a factor of two here, to stay consistent with the definition (13) above.

Let us define $\tilde{u}_t = u_t L^{y_t}$, $\tilde{u}_h = u_h L^{y_h}$, and $\tilde{u}_i = u_i L^{y_i}$. Now let us compute the second partial derivative of f with respect to h at $h = 0$:

$$\left. \frac{\partial^2 f}{\partial h^2} \right|_{h=0} = L^{-d} \left. \frac{\partial^2 \mathcal{F}_{sing}}{\partial h^2} \right|_{h=0} + \left. \frac{\partial^2 g}{\partial h^2} \right|_{h=0}, \quad (25)$$

where

$$\begin{aligned} L^{-d} \left. \frac{\partial^2 \mathcal{F}_{sing}}{\partial h^2} \right|_{h=0} &= \left. \frac{\partial \mathcal{F}_{sing}}{\partial \tilde{u}_t} \right|_{h=0} 2 (g_{12}(D) + \dots) L^{y_t-d} \\ &+ \left. \frac{\partial^2 \mathcal{F}_{sing}}{\partial \tilde{u}_h^2} \right|_{h=0} (g_{02}(D) [1 + g_{12}(D) t + \dots])^2 L^{2y_h-d} + \dots \end{aligned} \quad (26)$$

There are also contributions stemming from partial derivatives with respect to \tilde{u}_i . However these are related with correction exponents $\epsilon > 4$ and therefore play little role in the analysis of the data.

It remains to Taylor expand $\left. \frac{\partial^2 \mathcal{F}_{sing}}{\partial \tilde{u}_h^2} \right|_{h=0}$ and $\left. \frac{\partial \mathcal{F}_{sing}}{\partial \tilde{u}_t} \right|_{h=0}$ in \tilde{u}_i . We arrive at corrections that are proportional to L^{y_3} , L^{2y_3} , L^{3y_3} , ..., $L^{y_{NR}}$, $L^{y_{NR}+y_3}$, ..., $L^{y''}$, ... Note that for an improved model, all terms with y_3 in the exponent have a vanishing amplitude, since $u_3 = 0$. For an improved model, at the critical point we get

$$\chi_{h=0,t=0,D=D^*} = a L^{2y_h-d} \left[1 + c_{NR} L^{y_{NR}} + c'' L^{y''} + c_t L^{y_t-2y_h} + \dots \right] + b. \quad (27)$$

Note that $2y_h - d = 2 - \eta$. The analytic background b can be viewed as a correction with the RG-exponent $y_b = \eta - 2 \approx -1.962$, which is close to $y_{NR} = -2.02(1)$. Also the value of $y_t - 2y_h \approx -3.473$ is close to that of y'' .

The energy density, eq. (12), is given by the first derivative of the free energy with respect to t . At the critical point we get

$$\left. \frac{\partial f}{\partial t} \right|_{t=0,h=0} = \left. \frac{\partial \mathcal{F}_{sing}}{\partial \tilde{u}_t} \right|_{t=0,h=0} g_{01}(D) L^{y_t-d} + \left. \frac{\partial \mathcal{F}_{sing}}{\partial \tilde{u}_3} \right|_{t=0,h=0} g_{23}(D) L^{y_i-d} + \left. \frac{\partial g}{\partial t} \right|_{t=0,h=0}. \quad (28)$$

It remains to Taylor expand $\left. \frac{\partial \mathcal{F}_{sing}}{\partial \tilde{u}_t} \right|_{t=0, h=0}$ in \tilde{u}_i . We arrive at

$$E = E_0 + aL^{y_t-d} \left(1 + c_{NR}L^{y_{NR}} + c_3L^{y_3-y_t} + c''L^{y''} + \dots \right) \quad (29)$$

for an improved model at the critical point. Note that $y_3 - y_t \approx -2.278$ is only slightly smaller than y_{NR} .

C. Phenomenological Couplings

A cornerstone of our analysis are dimensionless quantities which are also called phenomenological couplings. In the following we shall denote them by R , since in our case they are ratios. The first quantity that we consider is the ratio of partition functions. We get

$$\ln \frac{Z_a}{Z_p} = V(f_p - f_a) = \mathcal{F}_{p,sing} - \mathcal{F}_{a,sing} , \quad (30)$$

since the analytic background exactly cancels. Hence

$$\frac{Z_a}{Z_p} = R_Z(L^{y_t}u_t, L^{y_h}u_h, \{L^{y_j}u_j\}) . \quad (31)$$

In addition we study the cumulants

$$U_{2j} = \frac{\langle m^{2j} \rangle}{\langle m^2 \rangle^j} \quad (32)$$

for $j = 2$ and 3 . Here we can build on the result obtained above for the magnetic susceptibility. Also $\langle m^{2j} \rangle$ can be computed from partial derivatives of the free energy density with respect to the external field h . The dominant contributions stem from the derivatives of the singular part of the free energy with respect to \tilde{u}_h and even derivatives of the singular part of the free energy with respect to \tilde{u}_t . Hence

$$U_{2j} = R_U(L^{y_t}u_t, L^{y_h}u_h, \{L^{y_i}u_i\}) + aL^{-2y_h+d} + bL^{-2y_h+y_t} + \dots . \quad (33)$$

In the case of the second moment correlation length ξ_{2nd} divided by the linear lattice size L we also expect corrections that go back to the magnetic susceptibility. In addition there is a correction $\propto L^{-2}$ due to the construction of ξ_{2nd} .

Taking the derivative of a phenomenological coupling with respect to the reduced temperature t we get

$$\left. \frac{\partial R}{\partial t} \right|_{h=0} = \left. \frac{\partial R}{\partial \tilde{u}_t} \right|_{h=0} (g_{01}(D) + g_{11}(D)t + \dots)L^{y_t} + \left. \frac{\partial R}{\partial \tilde{u}_3} \right|_{h=0} g_{23}(D)L^{y_3} + \dots . \quad (34)$$

At the critical point of an improved model

$$\left. \frac{\partial R}{\partial t} \right|_{t=0, h=0, D=D^*} = aL^{yt} \left(1 + cL^{yNR} + \dots + d g_{23} L^{-yt+y_3} + \dots \right), \quad (35)$$

where we performed a Taylor expansion of $\frac{\partial R}{\partial \tilde{u}_i}$ and $\frac{\partial R}{\partial \tilde{u}_3}$ with respect to $\{\tilde{u}_i\}$.

D. Fixing the value of R

In the analysis of our data, we consider certain quantities at a fixed value R_f of a dimensionless quantity. This means that for each lattice size L , we compute $\beta_f(D, L)$ defined by

$$R(\beta_f(D, L), D, L) = R_f. \quad (36)$$

Note that we have skipped the argument h , since $h = 0$ throughout. Making use of eq. (31) we get

$$R(\beta_f, D, L) = R^* + a(D)(\beta_c(D) - \beta)L^{yt} + \dots + c(D)L^{y_3} + \dots. \quad (37)$$

for $R_f \approx R^*$, where R^* is the fixed point value of R . Hence

$$\beta_f(D, L) = \beta_c(D) - a(D)^{-1}(R^* - R_f)L^{-yt} + \dots + a(D)^{-1}c(D)L^{y_3-yt} + a(D)^{-1}d(D)L^{yNR-yt} + \dots. \quad (38)$$

Note that $c(D^*) = 0$. First we consider a phenomenological coupling R_2 at a fixed value $R_{1,f}$ of an other phenomenological coupling R_1 . One gets

$$R_2(R_{1,f}, D, L) = r_2(R_{1,f}, \{\tilde{u}_i\}) + c(R_{1,f}, D)L^{y_3-yt} + \dots + d(D)L^{2y_3-yt} + \dots, \quad (39)$$

where $c(R_1^*, D) = 0$. Note that the corrections are due to the fact that the u_i depend on t , see eq. (22).

We also compute the magnetic susceptibility and the slope of phenomenological couplings at R_f . Plugging in eq. (38) into eqs. (26, 34) we see that compared with eqs. (27,35) additional correction terms proportional to $(R_f - R^*)L^{-yt}$, $(D - D^*)L^{-yt+y_3}$ and $L^{-yt+yNR}$ appear. Therefore it is favorable to take $R_f \approx R^*$. In the numerical analysis, one should vary R_f to check the effect of a possible deviation from R^* .

IV. THE ALGORITHM

As in previous studies, for example refs. [12, 16], we have implemented a hybrid of local Metropolis updates, the single cluster update [32], and the wall cluster update [22]. Now let us discuss in detail these components of the algorithm and their implementation.

A. Local Metropolis algorithm

As usual, in the elementary step of the local update, the variable at a single site is changed, while all other variables are kept fixed. Using these elementary updates, we go through the lattice in typewriter fashion. Going through the lattice once is called a sweep. We use two different ways to generate the proposal for the local Metropolis update. In both cases, the proposal $\{\vec{s}\}'$ is accepted with the probability

$$P_{acc} = \min[1, \exp(-\Delta H)] , \quad (40)$$

where

$$\Delta H = H(\{\vec{s}\}') - H(\{\vec{s}\}) . \quad (41)$$

The weight, eq. (7), is taken into account by the probabilities used to generate the proposal. The first choice is given by the following probabilities: If $\vec{s}_x = (0, 0)$ we take with equal probability one of the N values with $|\vec{s}'_x| = 1$ as proposal. Else, for $|\vec{s}_x| = 1$, we always take $\vec{s}'_x = (0, 0)$ as proposal.

For an efficient implementation, one should avoid to compute $\exp(\cdot)$ for each update step. Instead we should store possible results in a table before the actual simulation is started.

The sum of all nearest neighbor spins can take a too large number of possible values to store $\exp(-\Delta H)$ efficiently. Therefore we tabulate instead the contribution to the Boltzmann factor by pairs

$$B(m, n) = \exp(\beta \vec{s}(m) \cdot \vec{s}(n)) \quad (42)$$

and its inverse $B^{-1}(m, n)$. Furthermore $\exp(-D)$ and $\exp(D)$ are computed once and are then stored. Then, for $m_x = 0$, where x is the site to be updated, we get

$$\exp(-\Delta H) = \exp(D) \prod_{y.nn.x} B(m'_x, m_y) , \quad (43)$$

where the product runs over all nearest neighbors (nn) of x . Note that $B(0, n) = 1$ for all values of n . For $m_x > 0$ we get

$$\exp(-\Delta H) = \exp(-D) \prod_{y.nn.x} B^{-1}(m_x, m_y) . \quad (44)$$

Since we were not able to prove the ergodicity of this algorithm, we used in addition a second choice of the proposal. It is generated independently of the old value of the variable. With probability $1/2$ we take $\vec{s}'_x = (0, 0)$ and with equal probabilities $1/(2N)$ one of the remaining values is chosen. Here

$$\exp(-\Delta H) = \exp(-D[\vec{s}_x^2 - \vec{s}'_x{}^2]) \prod_{y.nn.x} [B^{-1}(m_x, m_y)B(m'_x, m_y)] . \quad (45)$$

This update costs more CPU time than the first. However ergodicity is obvious.

B. Cluster algorithms

Cluster algorithms can be applied without major modifications compared with the ddXY model. We just have to note that the reflection has to be chosen such that the field variables remain in the allowed set of values. A reflection is given by

$$\vec{s}' = \vec{s} - 2(\vec{r} \cdot \vec{s})\vec{r} , \quad (46)$$

where

$$\vec{r} = (\cos(\pi m/N), \sin(\pi m/N)) \quad (47)$$

with $m = 0, 1, 2, \dots, N - 1$. The cluster update is characterized by the delete probability

$$p_d(\vec{s}_x, \vec{s}_y) = \min [1, \exp(-2\beta[\vec{r} \cdot \vec{s}_x][\vec{r} \cdot \vec{s}_y])] . \quad (48)$$

The values of p_d are tabulated before the actual simulation is started. For a discussion of the single cluster [32] and the wall cluster update [22] used for the simulation of the ddXY model see [12, 16].

C. The implementation

Our simulations are organized in a similar fashion as in [12, 16]. Since we could not store the results of all measurements on hard disc, we performed a binning of the data during the simulation.

During the study we varied the precise composition of the update cycle. In most of the simulations the following cycle, given by a C-code, is used:

```
for(i=0;i<N_bin;i++)
{
Metropolis_2();
for(k=0;k<6;k++)
{
Metropolis_1();
for(j=0;j<L;j++) single_cluster();
Metropolis_1();
wall_cluster(direction=k%3);
measurements();
}
}
```

Here `Metropolis_1()` and `Metropolis_2()` are sweeps, using the first and second type of the Metropolis update discussed in section IV A. The single cluster update is given by `single_cluster()` and `wall_cluster(direction=k%3)` is a wall cluster update for one of the three spacial directions. The plane is perpendicular to the k -axis. The position of the plane is randomly chosen in $\{0, 1, 2, \dots, L - 1\}$. In order to compute Z_a/Z_p we need two subsequent wall cluster updates, where the two reflection axes are perpendicular. The first axis is chosen randomly among the N possible directions.

We did run our program on standard x86 CPUs. For lack of human time, we made no attempt to implement our program on a graphics processing unit (GPU). For cluster algorithms on GPUs see for example refs. [37, 38].

Let us briefly comment on the CPU time required by the different components of the update cycle. We performed the simulations on various PCs and servers at the institute of theoretical physics. Here we quote numbers for a single core of an Intel(R) Xeon(R) CPU E3-1225 v3 running at 3.20 GHz. We implemented the code in standard C and used the SIMD-oriented Fast Mersenne Twister algorithm [39] as random number generator.

Our Metropolis update type one requires 1.2×10^{-8} s per site. In the case of the single cluster update about 3.8×10^{-8} s per site are needed. Note that the random number

generator requires for one sequential access about 3×10^{-9} s. Compared with our program for the ddXY model, these updates are faster by roughly a factor of three.

Plots were generated by using the Matplotlib library [40]. The least square fits were performed by using the function `curve_fit()` contained in the SciPy library [41] with the default Levenberg-Marquardt algorithm [42–44]. The function `curve_fit()` acts as a wrapper to functions contained in the MINPACK library [45].

V. THE SIMULATIONS AND THE ANALYSIS OF THE DATA

We simulated the model for $N = 8$ at various values of D , close to the inverse critical temperature $\beta_c(D)$. Most CPU time is spent on simulations for $D = 1.02, 1.05,$ and 1.07 which are close to D^* . We simulated linear lattice sizes up to $L = 512$, where the statistics is decreasing with increasing L . In figure 1 we plot the number of measurements times the volume L^3 as a function of the linear lattice size L for $D = 1.05$ and 1.07 . In the case of $D = 1.02$ the statistics is similar but we have simulated at fewer lattice sizes in the range $L = 20$ up to 80 . In addition we simulated at $D = -0.7, -0.5, 0, 0.45, 0.9, 1.24,$ and ∞ . In these cases we considered linear lattice sizes up to $L = 64, 64, 72, 72, 48, 48,$ and 72 , respectively. The main purpose of these simulations is to determine the correction exponent ω . A few simulations at $D = -0.85, -0.86,$ and -0.87 are performed to obtain a rough estimate of the tricritical point.

Our simulations were performed on various PCs and servers. In total these simulations took the equivalent of about 50 years of CPU time on a single core of a Intel(R) Xeon(R) CPU E3-1225 v3 running at 3.20 GHz. Note that the study was not systematically designed at the start but grew with time, also depending on the availability of CPU time.

Let us briefly comment on the assessment of the error of the final estimates for critical exponents and other quantities of interest. In the ansätze we can take into account only a small number of correction terms. This inevitably leads to systematic errors caused by corrections to scaling that are not explicitly taken into account. A large $\chi^2/\text{d.o.f.}$ indicates that the ansatz is not adequate to represent the data. However, dealing with an ansatz that not fully represents the underlying function, a small $\chi^2/\text{d.o.f.}$ and a corresponding acceptable goodness of the fit says very little on the deviation of the fit parameters from their true values. In order to get some handle on systematic errors caused by corrections to

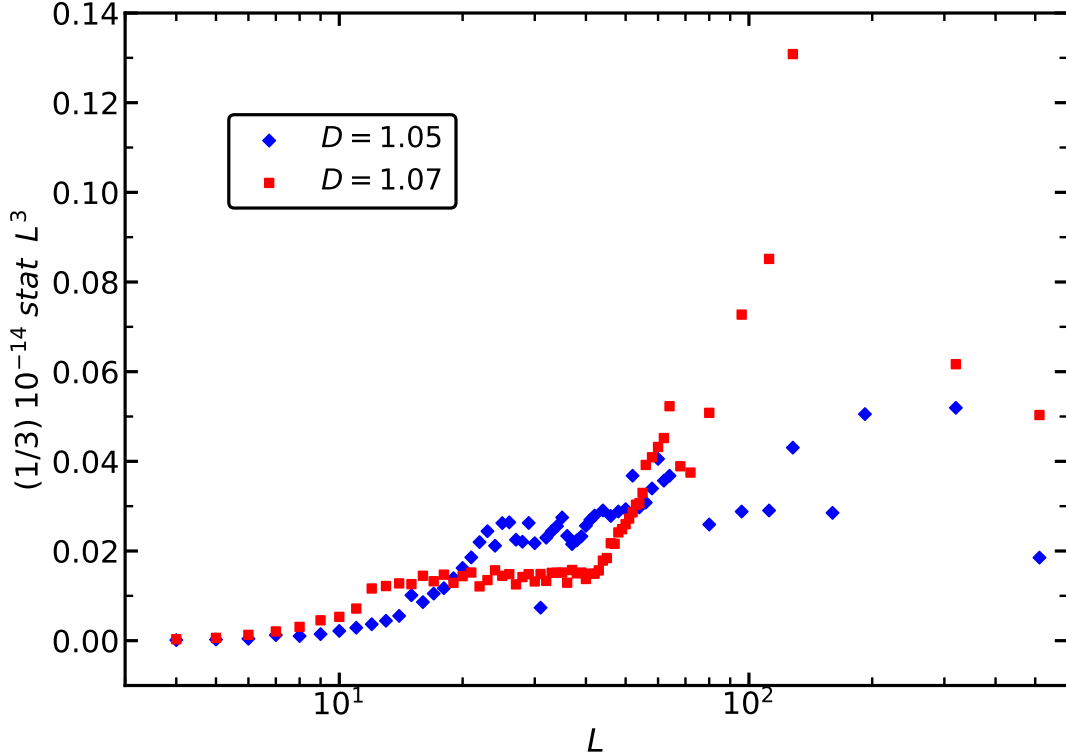


FIG. 1. We plot the number of measurements times the volume L^3 as a function of the linear lattice size L for $N = 8$ at $D = 1.05$ and $D = 1.07$.

scaling that are not taken into account in the ansatz, we either consider a number of different quantities or ansätze with a different number of correction terms. The final estimate and its error bar are chosen such that these different estimates are covered. The actual choice, which fits and minimal lattice sizes are taken into account, is at least partially an ad hoc decision. To allow the reader an own assessment, the direct outcome of fits is given in figures. We made no effort to give a separate estimate of the statistical and systematical error, since they are interwoven in our assessment.

The analysis of the data is organized in the following way: First we perform joint fits of our data for the dimensionless quantities R for $D = 1.02, 1.05$ and 1.07 . The results are the fixed point values R^* and estimates of the inverse critical temperatures. Next we include values of D with a larger amplitude of the leading correction to determine the exponent ω . To this end we analyze the cumulants U_4 and U_6 at a fixed values of either Z_a/Z_p or ξ_{2nd}/L . Then we determine D^* focusing again on $D = 1.02, 1.05$ and 1.07 . It follows a rough localization of the tricritical point D^* . In the final step of the analysis, we determine

the critical exponents ν and η . To this end we analyze the finite size scaling behavior the slopes of dimensionless quantities R , the energy density and the magnetic susceptibility.

A. The critical coupling β_c and the fixed point values of dimensionless ratios R^*

First we determined the critical coupling $\beta_c(D)$ and the fixed point values R^* of the dimensionless quantities that we have computed. To this end we analyzed our data at $D = 1.02, 1.05, \text{ and } 1.07$, which are close to D^* .

Motivated by eqs. (31,33), we have fitted our data with four different ansätze

$$R(L, D, \beta_c(D)) = R^* \quad , \quad (49)$$

$$R(L, D, \beta_c(D)) = R^* + b(D)L^{-\epsilon_1} \quad , \quad (50)$$

$$R(L, D, \beta_c(D)) = R^* + b(D)L^{-\epsilon_1} + c(D)L^{-\epsilon_2} \quad , \quad (51)$$

$$R(L, D, \beta_c(D)) = R^* + b(D)L^{-\epsilon_1} + c(D)L^{-\epsilon_2} + d(D)L^{-\epsilon_3} \quad . \quad (52)$$

We need the phenomenological couplings R as a function of the inverse temperature. To this end we have used the Taylor series around the value β_s of the inverse temperature used in the simulation. We have checked that β_c and β_s are sufficiently close to avoid significant truncation effects. This way, for example eq. (50) becomes

$$R(L, \beta_s) = R^* - c_1(L, \beta_s)(\beta_c - \beta_s) - \frac{c_2(L, \beta_s)}{2!}(\beta_c - \beta_s)^2 - \frac{c_3(L, \beta_s)}{3!}(\beta_c - \beta_s)^3 \quad , \quad (53)$$

where R^* and β_c are the two parameters of the fit.

It turned out that fits with the ansatz (50) are not very useful, since the amplitude of leading corrections is small for the values of D considered here. Therefore we shall not discuss the results of these fits in the following. Furthermore we did not consider ansätze with $\epsilon_2 = 2\omega$ here, since the amplitude of such corrections should be very small. This will be verified below in section VB. In the case of Z_a/Z_p we have used in eq. (51) the choices $\epsilon_1 = 0.79$ and $\epsilon_2 = 2.02$. In eq. (52) we used in addition either $\epsilon_3 = 3.5$ or $\epsilon_3 = 4$. Note that below, in section VB, we shall find $\omega = 0.789(4)$, eq. (59).

We performed a preliminary analysis using different parameterizations and choices of data sets. Based on this analysis we decided to extract the final results in the following way: We performed joint fits for the three values $D = 1.02, 1.05, \text{ and } 1.07$, where we parameterize

the amplitude of the leading correction as

$$b(D) = b_s(D - D^*) \quad (54)$$

and the amplitudes of higher corrections, $c(D)$ and $d(D)$ are assumed to be the same for all three values of D .

First we analyzed the data for the ratio of partition functions Z_a/Z_p . In figure 2 we plot results for $(Z_a/Z_p)^*$ of fits using the ansätze (49,51,52). We give only data points with $\chi^2/\text{d.o.f.} < 4$. In the case of ansatz (49) we see that $\chi^2/\text{d.o.f.}$ decreases rapidly with increasing L_{min} , where L_{min} is the minimal lattice size that is included into the fit. For $L_{min} = 33$, $\chi^2/\text{d.o.f.} = 1.012$ is reached. For ansatz (51) we find $\chi^2/\text{d.o.f.} = 0.986$ already for $L_{min} = 9$. As amplitude of the correction $\propto L^{-2.02}$ we find $c \approx -0.07$. For ansatz (52) with $\epsilon_3 = 4$ we find $\chi^2/\text{d.o.f.} = 0.972$ for $L_{min} = 5$. The amplitude of the correction $\propto L^{-4}$ is $d \approx -1.6$. Consistently with ansatz (51) find $c \approx -0.06$. Using $\epsilon_3 = 3.5$ instead, we get $\chi^2/\text{d.o.f.} = 1.135$ for $L_{min} = 5$ and $\chi^2/\text{d.o.f.} = 0.889$ for $L_{min} = 7$. For $L_{min} = 7$ we get $d = -0.85(4)$ and $c = -0.028(5)$. The fact that the amplitude of the correction $\propto L^{-\epsilon_3}$ is much larger than that of $\propto L^{-2.02}$ is surprising.

Our final estimate

$$(Z_a/Z_p)^* = 0.32037(6) \quad (55)$$

is taken such that it is consistent with the results of the three different ansätze. Note that we also varied the values of ϵ_1 and ϵ_2 within the range of the expected error bars. The results of the fits change little. In a similar way we arrive at the estimates for D^* and β_c at $D = 1.02, 1.05$ and 1.07 . These estimates are given in table III.

Next we analyzed the data for the ratio ξ_{2nd}/L and the cumulants U_4 and U_6 in a similar way, taking into account that also corrections $\propto L^{\eta-2}$ might be present. The final results are summarized in table III.

The estimates for R^* can be compared with $(Z_a/Z_p)^* = 0.3203(1)[3]$, $(\xi_{2nd}/L)^* = 0.5924(1)[3]$, $U_4^* = 1.2431(1)[1]$, and $U_6^* = 1.7509(2)[7]$ given in table I of [12]. These results were obtained by analyzing data obtained for the 2-component ϕ^4 and the ddXY model on the simple cubic lattice. In ref. [12] the authors tried to distinguish between statistical $(\)$ and systematical \square error. We find a nice agreement of the estimates, giving support to the hypothesis that the improved (8+1)-state clock model shares the three-dimensional XY universality class.

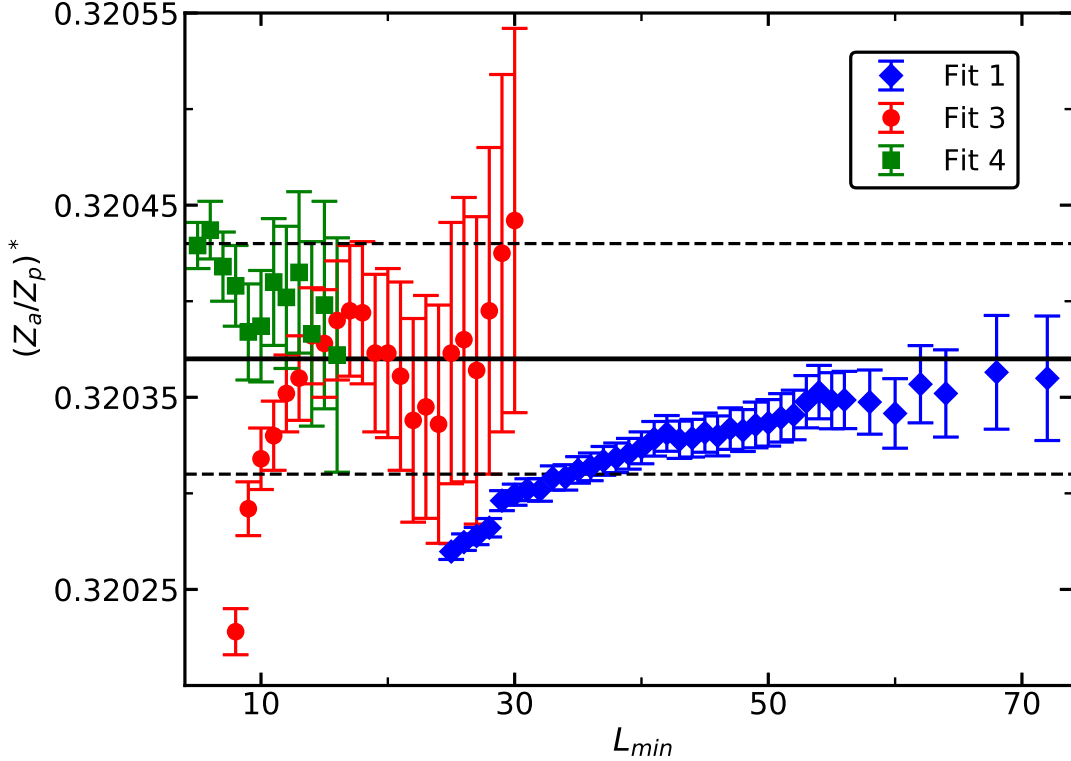


FIG. 2. We give the results for $(Z_a/Z_p)^*$ fitting with the ansätze (49,51) and (52) with $\epsilon_3 = 4$, corresponding to fit 1, 3, and 4 in the legend of the figure, as a function of the minimal lattice size L_{min} that is included in the fit. Data for $D = 1.02, 1.05$ and 1.07 are jointly fitted. The solid line gives our final estimate and the dashed ones the corresponding error.

The estimates of D^* and β_c obtained from U_4 and U_6 are the same up to the digits given here. In contrast, the differences with the estimates obtained from Z_a/Z_p and ξ_{2nd}/L are of similar size as the statistical errors. These differences are likely due to subleading corrections that are not taken into account in the ansätze. We find that the error of D^* obtained from Z_a/Z_p or ξ_{2nd}/L is larger than that of D^* obtained from U_4 or U_6 . Below in section VB 2 we give our final estimate of D^* . In the last row of table III we give our final estimates of β_c , which are mainly based on the analysis of Z_a/Z_p and ξ_{2nd}/L . The error bars are chosen such that the estimates obtained from Z_a/Z_p and ξ_{2nd}/L , including their error bars are covered. For the inverse critical temperature at the remaining values of D see Appendix A.

TABLE III. In the first column the phenomenological coupling is specified. In the second column we give the corresponding estimates of the fixed point values R^* . In the third column we give the estimates of D^* , where leading corrections to scaling vanish. In the following columns, the estimates of the inverse critical temperature β_c for $D = 1.02, 1.05,$ and 1.07 are given. These estimates are based on joint fits of our data for $D = 1.02, 1.05,$ and $1.07,$ as discussed in the text. In the last row we give our final estimates of β_c .

R	R^*	D^*	$\beta_c(1.02)$	$\beta_c(1.05)$	$\beta_c(1.07)$
Z_a/Z_p	0.32037(6)	1.065(35)	0.56379620(8)	0.56082390(7)	0.55888342(7)
ξ_{2nd}/L	0.59238(7)	1.075(25)	0.56379622(9)	0.56082391(8)	0.55888342(8)
U_4	1.24296(8)	1.054(10)	0.56379626(8)	0.56082386(8)	0.55888335(10)
U_6	1.75040(25)	1.054(10)	0.56379626(8)	0.56082386(8)	0.55888335(10)
			0.56379622(10)	0.56082390(10)	0.55888340(10)

B. Corrections to scaling

In this section we focus on corrections to scaling. To this end it is useful to consider the cumulants U_4 and U_6 at a fixed value of Z_a/Z_p or ξ_{2nd}/L [22]. In particular we take $Z_a/Z_p = 0.32037$ and $\xi_{2nd}/L = 0.59238$, which are our estimates of the fixed point values of these quantities. This means that U_4 and U_6 are taken at β_f , where β_f is chosen such that either $Z_a/Z_p = 0.32037$ or $\xi_{2nd}/L = 0.59238$. In the following we denote a cumulant at a fixed value of Z_a/Z_p or ξ_{2nd}/L by \bar{U} . Taylor expanding eq. (39) we get

$$\bar{U} = \bar{U}^* + b(D)L^{-\omega} + cb^2(D)L^{-2\omega} + \dots + d(D)L^{-\omega_2} + \dots \quad (56)$$

$$+[f(R_f - R^*) + g(D - D^*)]L^{-1/\nu-\omega} + \dots, \quad (57)$$

where R denotes either Z_a/Z_p or ξ_{2nd}/L . Note that here f and g are coefficients and not functions.

In figure 3, as a first step of the analysis, we plot U_4 at $Z_a/Z_p = 0.32037$ for $D = 0.45, 0.9, 1.05, 1.24$ and ∞ . We have omitted $D = 1.02$ and 1.07 to keep the figure readable. For $D = 1.05$ we see very little dependence of \bar{U}_4 on L , which confirms that $D = 1.05$ is close to D^* . For $D = \infty$ we find that \bar{U}_4 is increasing with increasing lattice size. It is approaching the curve for $D = 1.05$. For $D = 0.45$ we see that \bar{U}_4 is decreasing and the amplitude of the

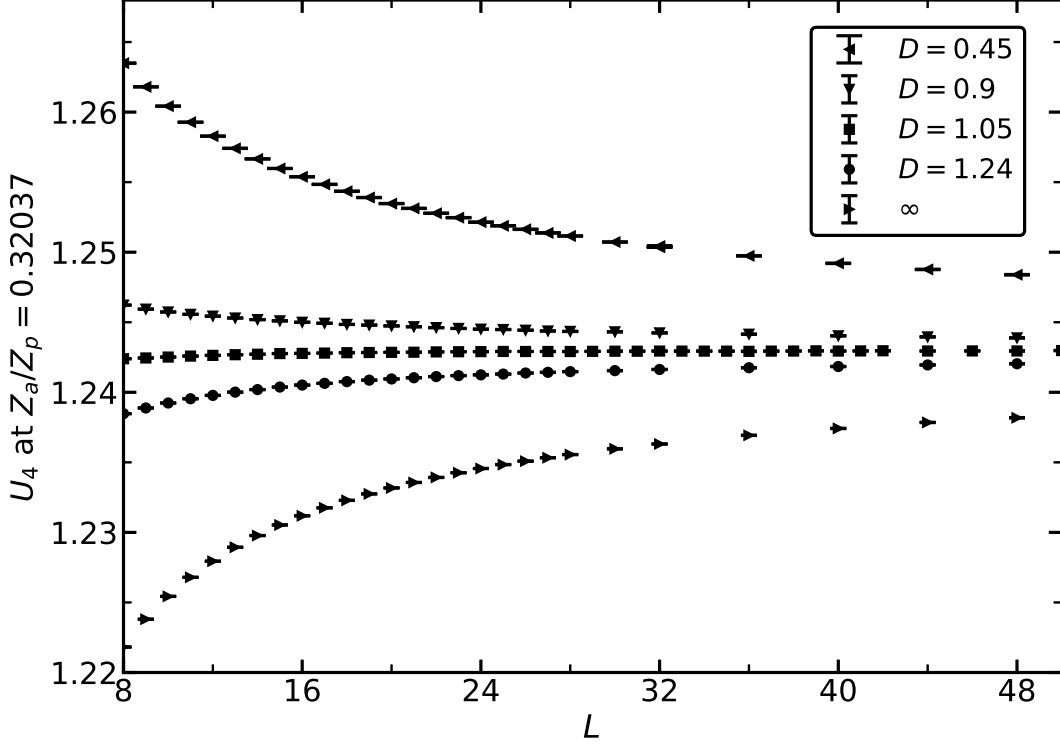


FIG. 3. We plot U_4 at $Z_a/Z_p = 0.32037$ for $N = 8$ at $D = 0.45, 0.9, 1.05, 1.24,$ and ∞ as a function of the linear lattice size L .

corrections is roughly equal to that at $D = \infty$, but with the opposite sign. Next in figure 4 we plot U_4 at $Z_a/Z_p = 0.32037$ for $D = -0.7, -0.5, 0,$ and 0.45 . Going to smaller values of D , much larger amplitudes of the leading correction can be obtained than for $D \rightarrow \infty$. Still for $D = -0.7$, where the amplitude of the corrections is the largest, the fixed point value is approached as the lattice size increases. This indicates that $D = -0.7$ is on the line of second order phase transitions. Below we shall study the tricritical point, which is located at a smaller value of D .

In the following we determine the exponent of the leading corrections ω and D^* , the value of D , where the amplitudes of leading corrections vanish.

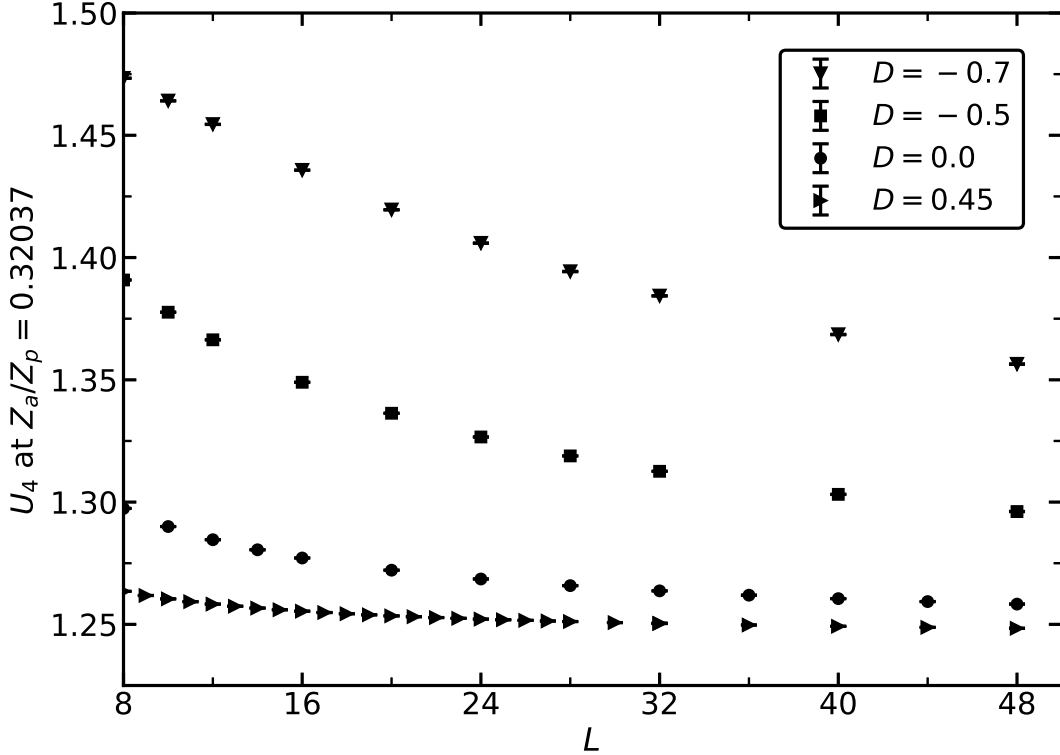


FIG. 4. We plot U_4 at $Z_a/Z_p = 0.32037$ for $N = 8$ at $D = 0.45, 0.0, -0.5,$ and -0.7 as a function of the linear lattice size L .

1. The correction exponent ω

We performed joints fits of our data for $D = -0.7, -0.5, 0.0, 0.45, 0.9, 1.02, 1.05, 1.07, 1.24,$ and ∞ . We used the ansatz

$$\bar{U} = \bar{U}^* + \sum_{i=1}^{i_{max}} c_i [b(D)L^{-\omega}]^i + dL^{-\epsilon}. \quad (58)$$

In order to avoid ambiguity, we set $c_1 = 1$. In most of our fits we used $\epsilon = 2$. Furthermore, it is assumed that d does not depend on D . At least for corrections due to the breaking of the rotational invariance this should be a good approximation. As a check, we also performed fits without the term $dL^{-\epsilon}$. Since our final results are taken from fits with $L_{min} \geq 16$, the term $dL^{-\epsilon}$ has only a small effect. The free parameters of our fits are $\bar{U}^*, b(D), c_i, \omega,$ and d .

First we fitted all data for all values of D listed above that satisfy $L \geq L_{min}$. Here we performed fits with $i_{max} = 2, 3, 4, 5, 6$. It turns out that the results for $\bar{U}_4^*, \bar{U}_6^*,$ and ω depend on i_{max} . Let us focus the discussion on ω , which is the most important quantity.

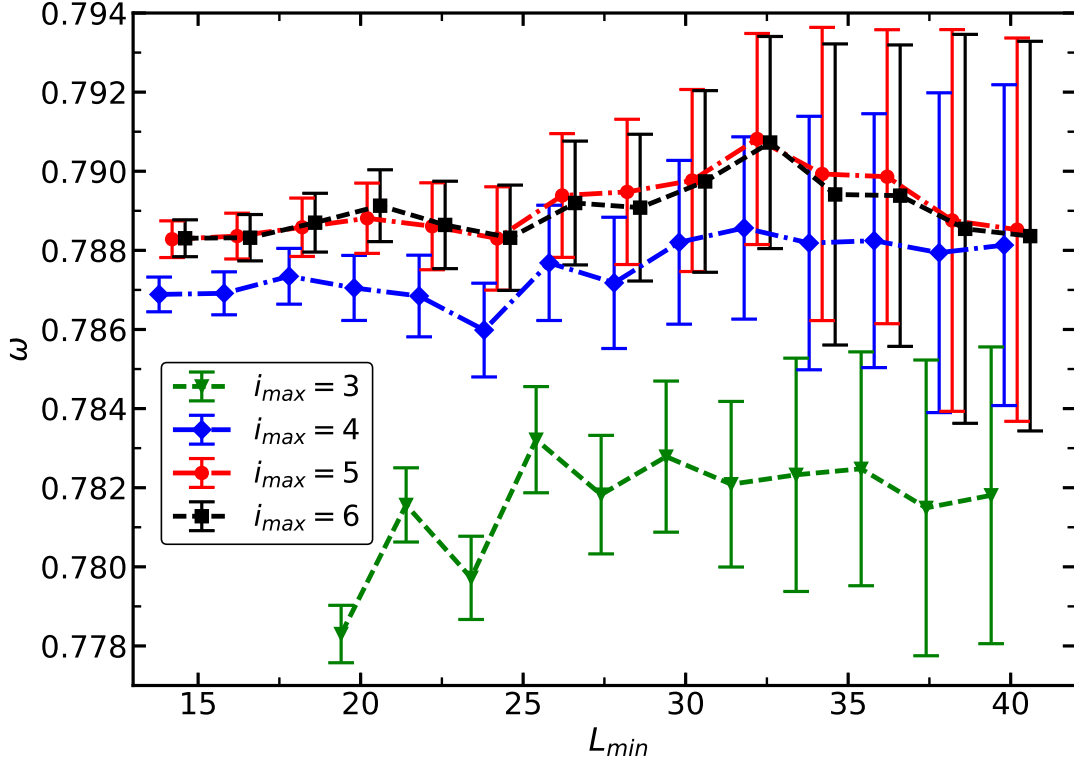


FIG. 5. We plot the estimates of the correction exponent ω obtained by fitting U_4 at $Z_a/Z_p = 0.32037$ using the ansatz (58), where all linear lattice sizes with $L_{min} \leq L$ are included. Data for $N = 8$ at $D = -0.7, -0.5, 0.0, 0.45, 0.9, 1.02, 1.05, 1.07, 1.24,$ and ∞ are taken into account. The lines connecting the data points should only guide the eye. The L_{min} are slightly shifted for different fits to make the figure readable.

In figure 5 we plot the results obtained from fits with $i_{max} = 3, 4, 5,$ and 6 of U_4 at $Z_a/Z_p = 0.32037$. We see that the estimates of ω are increasing with increasing i_{max} . For $i_{max} = 5$ and 6 the values saturate. In the plot we give only results that correspond to $\chi^2/\text{d.o.f.} < 4$. With increasing L_{min} the $\chi^2/\text{d.o.f.}$ rapidly converge to $\chi^2/\text{d.o.f.} \approx 1$. As our intermediate result of this set of fits, we take $\omega = 0.7886(11)$ from $i_{max} = 5$ and 6 at $L_{min} = 22$. Performing a similar analysis for U_6 at $Z_a/Z_p = 0.32037$, we arrive at $\omega = 0.7880(11)$.

As a check, we have repeated the analysis including fewer values of D : $D = 0.45, 0.9, 1.02, 1.05, 1.07, 1.24,$ and ∞ . Note that for $D = 0.45$ the amplitude of leading corrections to scaling is, up to the sign, roughly the same as for $D = \infty$. Since we have skipped the data with a large amplitude of corrections to scaling, already fits with $i_{max} = 2$ are consistent with

fits using $i_{max} = 3$. As intermediate results we quote $\omega = 0.7896(8)$ for U_4 and $L_{min} = 18$ and $\omega = 0.7886(8)$ for U_6 and $L_{min} = 18$.

Next we analyzed U_4 and U_6 at $\xi_{2nd}/L = 0.59238$. Our intermediate results for ω are slightly smaller than those obtained above. Furthermore we see a stronger dependence of the results on L_{min} .

Taking all 10 values of D and $L_{min} = 26$ we get $\omega = 0.7870(14)$ for U_4 and $0.7862(14)$ for U_6 as intermediate result. Using only $D \geq 0.45$ we get $\omega = 0.7883(21)$ for $L_{min} = 30$ from U_4 and $i_{max} = 2$. Based on U_6 we arrive at $\omega = 0.7875(20)$.

As our final value we quote

$$\omega = 0.789(4) \quad . \quad (59)$$

The central value is mainly given by the results obtain from U_4 and U_6 at $Z_a/Z_p = 0.32037$, since here the estimates depend less on L_{min} than it is the case for fixing $\xi_{2nd}/L = 0.59238$. The error bar is chosen such that also the intermediate results obtain for fixing $\xi_{2nd}/L = 0.59238$ are covered.

2. Locating D^*

Next we estimate the value D^* of D , where leading corrections to scaling vanish. To this end, we focus again on the neighborhood of D^* and include only data for $D = 1.02, 1.05$, and 1.07 into the analysis. Since the values of $b(D)$ are small, we have omitted terms with $L^{-n\omega}$ and $n \geq 2$. We made no attempt to discriminate the terms $L^{2-\eta}$ and $L^{-\omega_{NR}}$ in our fits. Hence we used a single term with an exponent $\epsilon_2 \approx 2$. We used the ansätze

$$\bar{U}(L, D) = \bar{U}^* + b(D)L^{-\epsilon_1} \quad , \quad (60)$$

$$\bar{U}(L, D) = \bar{U}^* + b(D)L^{-\epsilon_1} + c(D)L^{-\epsilon_2} \quad , \quad (61)$$

$$\bar{U}(L, D) = \bar{U}^* + b(D)L^{-\epsilon_1} + c(D)L^{-\epsilon_2} + d(D)L^{-\epsilon_3} \quad . \quad (62)$$

Since the values of D differ little, we performed fits where c and d are the same for all values of D . Furthermore $b(D) = b'(D - D^*)$, where b' and D^* are the free parameters.

First we analyzed U_4 at $Z_a/Z_p = 0.32037$. We performed fits without subleading corrections, with one subleading correction term and with two subleading correction terms. In the case of one subleading correction term we used the two choices $\epsilon_2 = 1.962$ and $\epsilon_2 = 2.02$

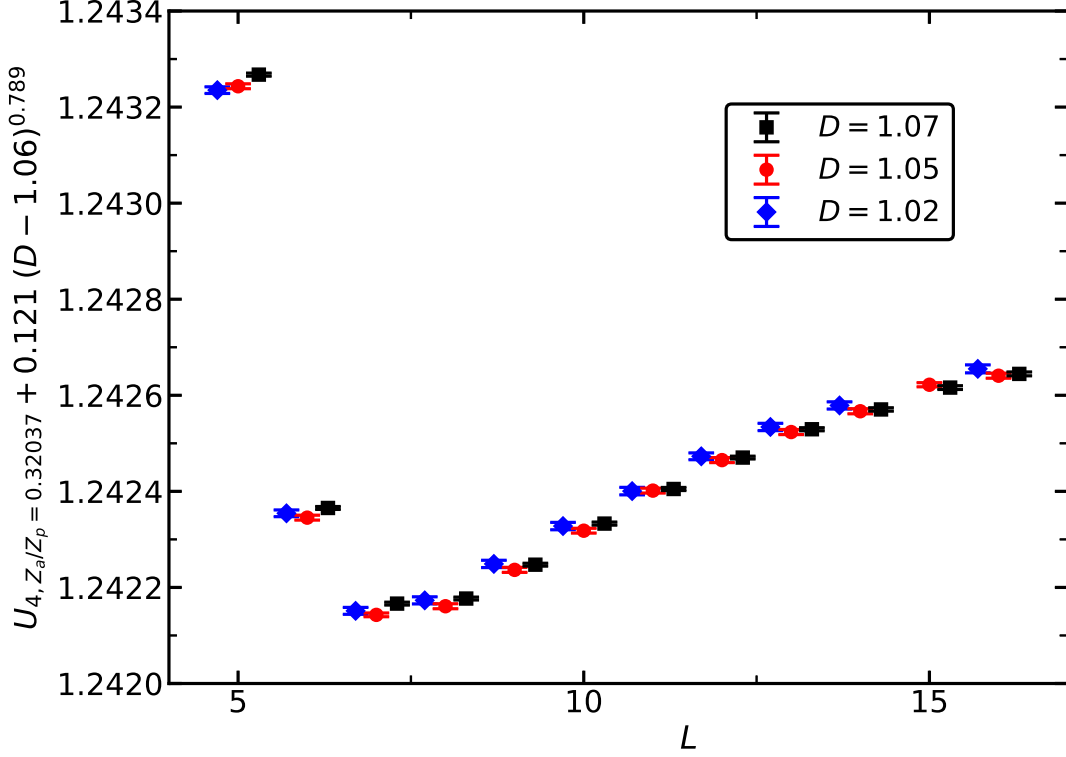


FIG. 6. We plot $U_4(Z_a/Z_p = 0.32037) + 0.121(D - 1.06)L^{-0.789}$ for $N = 8$ at $D = 1.02, 1.05,$ and 1.07 . Note that we have shifted the values of L for $D = 1.02$ and 1.07 to make the figure readable.

Our estimate of the parameter b' for U_4 at $Z_a/Z_p = 0.32037$ and $\epsilon_1 = \omega = 0.789$ fixed is $b' = -0.121(5)$. In figure 6 we plot $\bar{U}_4 + 0.121(D - 1.06)L^{-0.789}$. We find that the data for $D = 1.02, 1.05,$ and 1.07 nicely collapse. This fact shows that our approximations of $b, c,$ and d are adequate.

In figure 7 we plot estimates of D^* obtained by fitting U_4 at $Z_a/Z_p = 0.32037$ with the ansätze (60,61,62).

Analyzing U_4 at $\xi_{2nd}/L = 0.59238$ we get a very similar result. Overall, the estimates of D^* are shifted by about 0.005 compared with $Z_a/Z_p = 0.32037$. As our final estimate we quote

$$D^* = 1.058(13) \tag{63}$$

that covers both the preliminary estimates obtained from fixing $Z_a/Z_p = 0.32037$ and $\xi_{2nd}/L = 0.59238$. For a discussion of the dependence of D^* on N see appendix B3.

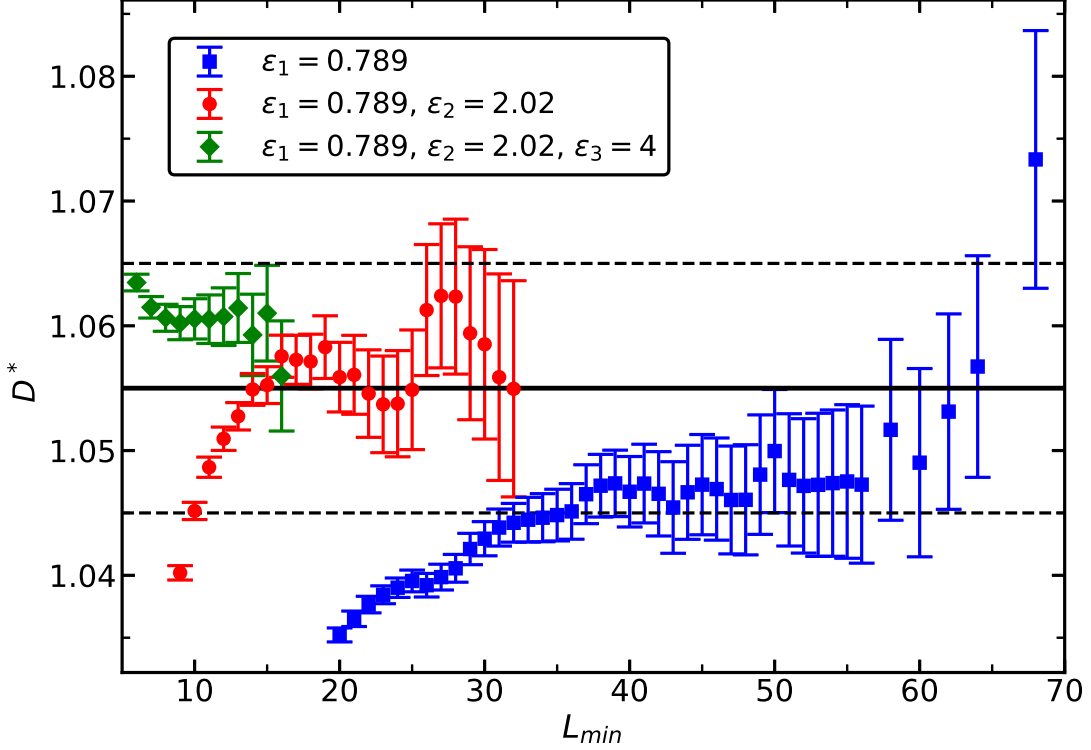


FIG. 7. We plot estimates of D^* obtained from fits of U_4 at $Z_a/Z_p = 0.32037$ for $N = 8$ at $D = 1.02, 1.05$, and 1.07 as a function of the minimal lattice size L_{min} taken into account. The ansätze (60,61,62) are used. The corresponding correction exponents are given in the legend. Our preliminary estimate $D^* = 1.055(10)$ is indicated by the straight solid line. The dashed lines give the error bar.

3. The tricritical point

The model undergoes a first order phase transition for $D < D_{tri}$. We performed preliminary simulations for a number of $D < D^*$ to roughly locate D_{tri} . In figure 8 we plot the Binder cumulant U_4 at $Z_a/Z_p = 0.32037$ for $D = -0.85, -0.86$, and -0.87 , which are close to our preliminary estimate of D_{tri} . For $D = -0.87$, the Binder cumulant is increasing with increasing lattice size for the lattice sizes studied. It seems plausible that this behavior extends to larger lattice sizes. In contrast, for $D = -0.86$, and more clearly for -0.85 , the Binder cumulant increases for small lattice sizes, while it decreases for larger ones. We conclude that $-0.87 < D_{tri} < -0.86$.

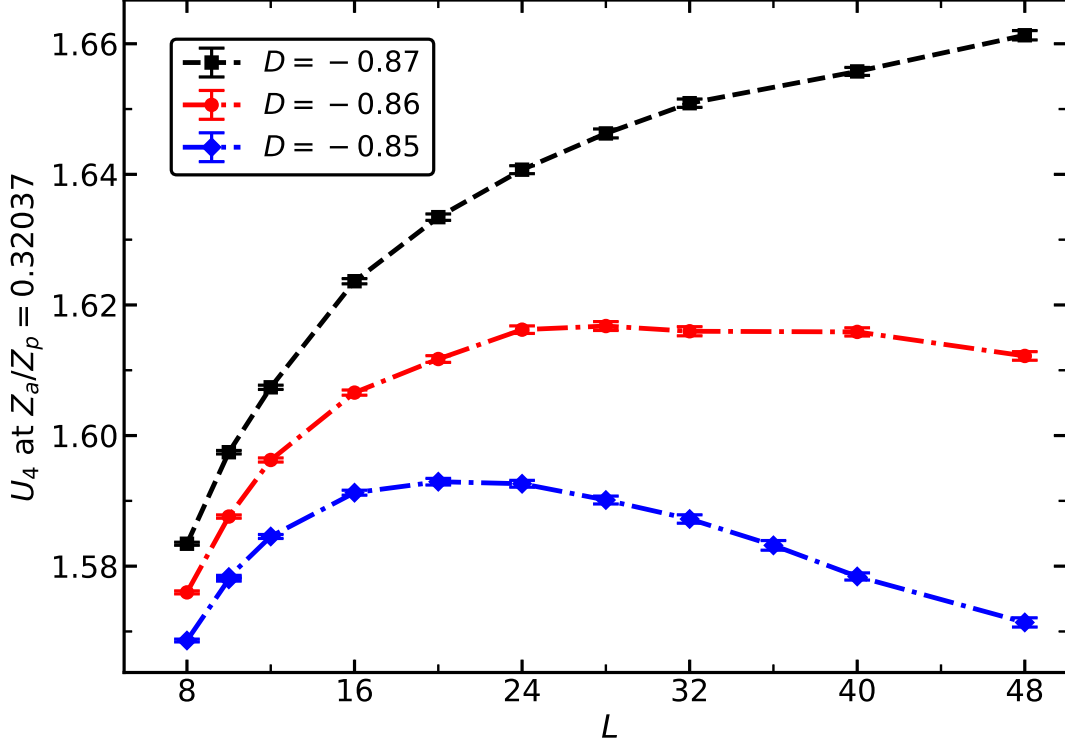


FIG. 8. We plot the Binder cumulant U_4 at $Z_a/Z_p = 0.32037$ for $N = 8$ at $D = -0.85, -0.86,$ and -0.87 for linear lattice sizes $8 \leq L \leq 48$. The lines connecting the data points should only guide the eye.

C. The critical exponent ν

We compute the exponent $\nu = 1/y_t$ from the derivative of a dimensionless quantity R_j with respect to β at a fixed value of a second quantity R_i , where R_j and R_i might be the same. Following the discussion of section III these slopes behave as

$$\bar{S}_{R,i,j} = \left. \frac{\partial R_j}{\partial \beta} \right|_{R_i=R_{i,f}} = aL^{y_t} [1 + bL^{-\omega} + \dots + cL^{-\omega_{NR}} + \dots] . \quad (64)$$

We construct improved slopes by multiplying $\bar{S}_{R,i,j}$ with a certain power p of the Binder cumulant \bar{U}_4 :

$$\bar{S}_{R,imp} = \bar{S}_R \bar{U}_4^p , \quad (65)$$

where both \bar{S}_R and \bar{U}_4 are taken at $R_{i,f}$. The exponent p is chosen such that, at the level of our numerical accuracy, leading corrections to scaling are eliminated. This idea is discussed systematically in ref. [26]. To determine p , we consider the pairs $(D_1, D_2) = (0.9, 1.24)$ and

TABLE IV. Numerical result for the exponents p that eliminate leading corrections to scaling in S_R , eq. (65).

Fixing \ Slope of	Z_a/Z_p	ξ_{2nd}/L	U_4	U_6
$Z_a/Z_p = 0.32037$:	0.95(3)	0.30(4)	-2.22(7)	-3.74(7)
$\xi_{2nd}/L = 0.59398$:	0.60(4)	0.41(4)	-2.36(6)	-3.86(6)

(0.45, ∞). These pairs are chosen such that the amplitude of leading corrections has roughly the same modulus, but opposite sign. We fit ratios of $\bar{S}_{R,i,j}$ and \bar{U}_4 with the ansätze

$$\frac{\bar{S}_{R,i,j}(D_1)}{\bar{S}_{R,i,j}(D_2)} = a_S(1 + b_S L^{-\epsilon_1}) \quad (66)$$

and

$$\frac{\bar{U}_4(D_1)}{\bar{U}_4(D_2)} = 1 + b_U L^{-\epsilon_1} , \quad (67)$$

where we fixed $\epsilon_1 = 0.789$. The exponent p is given by

$$p = -\frac{b_S}{b_U} . \quad (68)$$

In table IV we give our final results for p . These are taken from fits for $(D_1, D_2) = (0.9, 1.24)$ and $L_{min} = 18$. The statistical error is dominated by eq. (66). In table IV we give the statistical error only. Our numerical results obtained for $(D_1, D_2) = (0.45, \infty)$ are consistent. In the case of $(D_1, D_2) = (0.45, \infty)$ we also used fits with one additional correction term. Note that the results for the exponent p change very little when we vary ϵ_1 within the error bars of eq. (59).

As a check, we have computed the RG-exponent y_t for $D = \infty$ using the ansatz $\bar{S}_R = aL^{y_t} (1 + cL^{-2})$. Taking the data for $\bar{S}_{R,imp}$ we get estimates that are consistent with our final result obtained below. In contrast, fitting \bar{S}_R without improvement, the results differ clearly and depend on the dimensionless ratio R that is considered.

1. Statistical errors

In the case of the slopes S_R we find a moderate reduction of the statistical error when computed at $Z_a/Z_p = 0.32037$ or $\xi_{2nd}/L = 0.59238$ instead of $\beta \approx \beta_c$. It is of the order of

a few percent. In contrast, for the magnetic susceptibility that we discuss below, we find a significant reduction. The relative statistical error of the slope of Z_a/Z_p and ξ_{2nd}/L is roughly the same. For U_4 and U_6 for $L = 32$ it is about twice as large as for Z_a/Z_p and ξ_{2nd}/L . With increasing lattice size this ratio is shrinking. For $L = 512$ roughly a factor of 1.8 remains. In general, there is a degradation with increasing lattice size. For example, the product of statistics times the square of the relative statistical error increases for the slope of ξ_{2nd}/L by a factor of 2.4 going from $L = 32$ to 512. Since we performed a binning of the data during the simulation, we can not disentangle whether this is due to an increasing autocorrelation time or an increasing variance.

2. Our final estimate of y_t

The idea of using improved derivatives at $D \approx D^*$ is that leading corrections are highly suppressed and they can be ignored safely. In order to obtain our final estimate of ν we perform joint fits of our data obtained for $D = 1.05$ and $D = 1.07$. We use the ansätze

$$\bar{S}_R = a(D)L^{y_t} , \quad (69)$$

$$\bar{S}_R = a(D)L^{y_t}(1 + cL^{-\epsilon_1}) , \quad (70)$$

where $\epsilon_1 \approx 2$. This choice is motivated by the fact that we expect corrections with the exponents $2 - \eta$, $\omega_R \approx 2.02$, and $-y_t + \omega \approx 2.278$ and larger ones. Our final estimates are based on fits with a single correction exponent.

In figure 9 we give the results of such fits for fixing $\xi_{2nd}/L = 0.59238$. The results obtained from the slope of U_6 are not plotted, since they are similar to those of U_4 . For Z_a/Z_p we get $\chi^2/\text{d.o.f} = 0.871$ with $L_{min} = 15$. For ξ_{2nd}/L we get $\chi^2/\text{d.o.f} = 1.000$ with $L_{min} = 20$. For U_4 we get $\chi^2/\text{d.o.f} = 0.815$ already for $L_{min} = 7$. The estimates of y_t obtained from the improved slopes of the three different quantities are consistent starting from $L_{min} \approx 18$. Furthermore the estimates are increasing with increasing L_{min} up to about $L_{min} = 23$. For $L_{min} = 23$, from the slopes of Z_a/Z_p and ξ_{2nd}/L we read off our preliminary result $y_t = 1.48878(12)$.

In figure 10 we give the results of such fits for fixing $Z_a/Z_p = 0.32037$. In the case of ξ_{2nd}/L we get $\chi^2/\text{d.o.f} = 1.064$ for $L_{min} = 15$. For Z_a/Z_p we get $\chi^2/\text{d.o.f} = 0.963$ with $L_{min} = 10$. In the case of U_4 we get $\chi^2/\text{d.o.f} = 0.899$ for $L_{min} = 8$. Despite this fact, fully

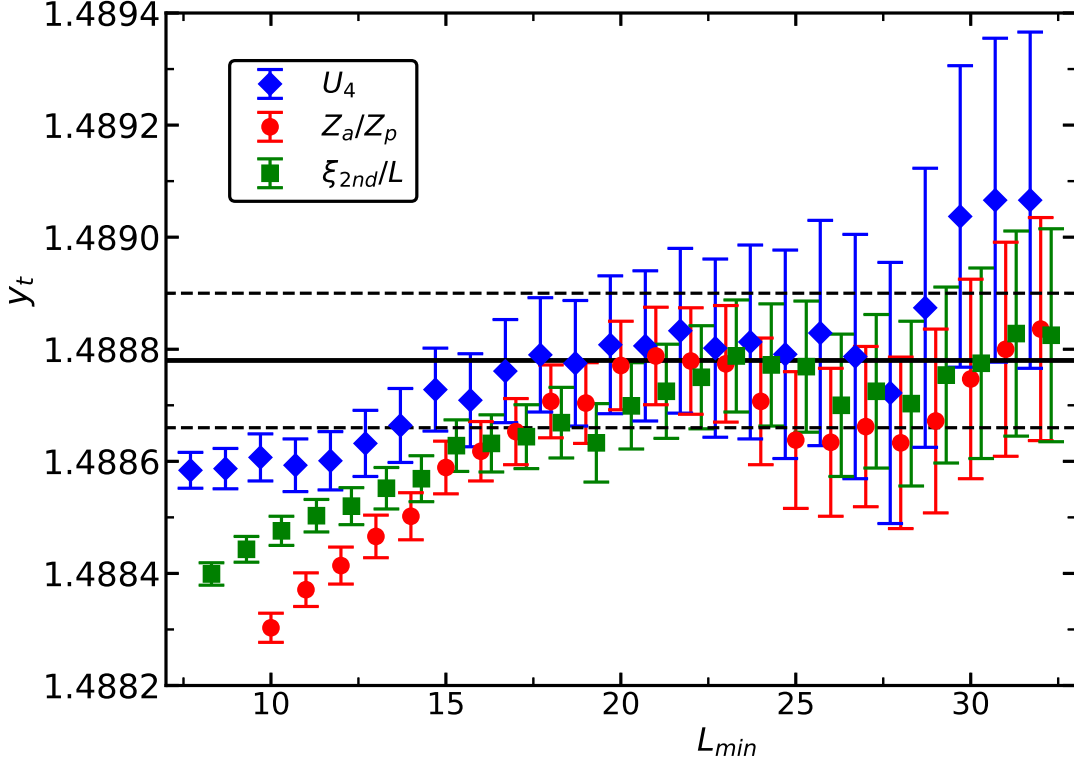


FIG. 9. Estimates of the RG-exponent y_t obtained from fitting the improved slopes of U_4 , Z_a/Z_p , and ξ_{2nd}/L at $\xi_{2nd}/L = 0.59238$ for $N = 8$ at $D = 1.05$ and 1.07 as a function of the minimal linear lattice size L_{min} that is taken into account. The ansatz (70) is used. To make the figure readable we shifted the values of L_{min} by -0.3 and 0.3 , for two of the fits. The straight solid line gives our preliminary estimate obtained from the improved slopes at $\xi_{2nd}/L = 0.59238$. The dashed lines indicate our preliminary error estimate.

consistent results for y_t among the three quantities are only reached for $L_{min} \approx 23$. Our preliminary result $y_t = 1.48880(13)$ is based on the fits of the slope of Z_a/Z_p and ξ_{2nd}/L for $L_{min} = 23$. In figure 10 it is indicated by a straight line. The dashed lines give our estimate of the error.

Taking into account both the results from fixing $\xi_{2nd}/L = 0.59238$ and $Z_a/Z_p = 0.32037$ we arrive at

$$y_t = 1.48879(14) . \quad (71)$$

The error bar covers both preliminary estimates, including their respective error bars. For the critical exponent of the correlation length we quote $\nu = 0.67169(7)$. We repeated

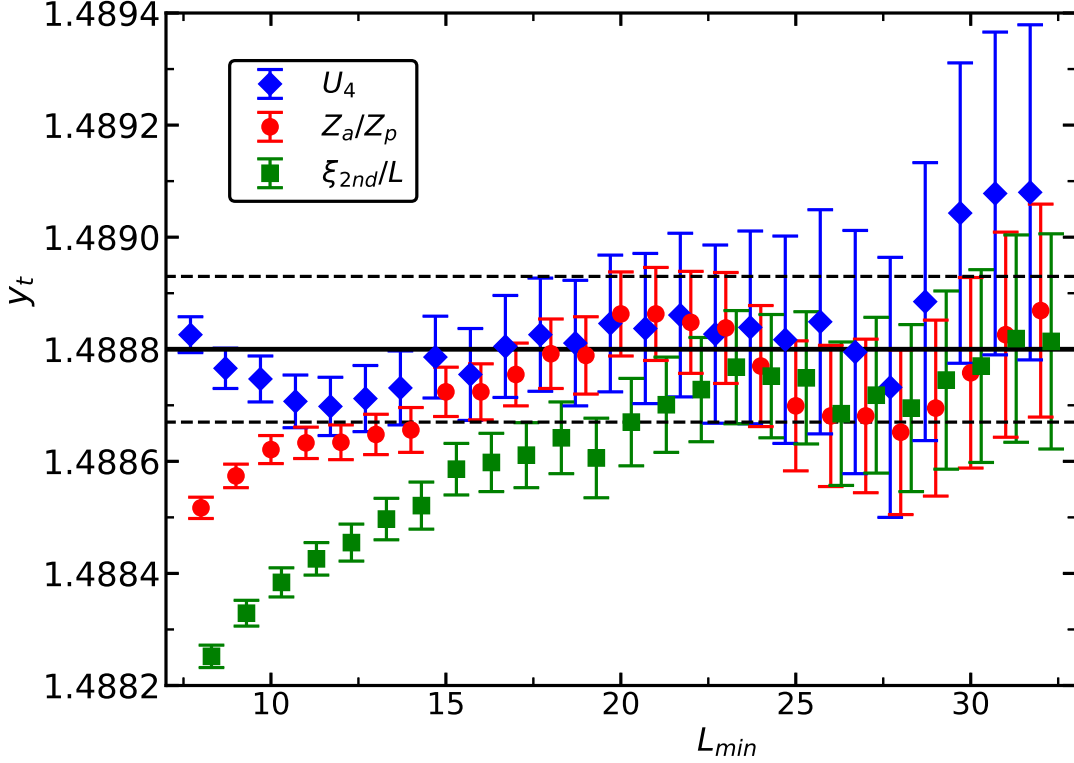


FIG. 10. Estimates of the RG-exponent y_t obtained from fitting the improved slopes of U_4 , Z_a/Z_p , and ξ_{2nd}/L at $Z_a/Z_p = 0.32037$ for $N = 8$ at $D = 1.05$ and 1.07 as a function of the minimal linear lattice size L_{min} that is taken into account. The ansatz (70) is used. To make the figure readable we shifted the values of L_{min} by -0.3 and 0.3 , for two of the fits. The straight lines indicate our preliminary result and its error estimate.

the fits using the ansatz (70) for fixing $Z_a/Z_p = 0.32$ and 0.321 and $\xi_{2nd}/L = 0.592$ and $\xi_{2nd}/L = 0.593$. The variation of the results for y_t is well below the error quoted in eq. (71).

Finally, in figure 11 we show results obtained from fits without corrections (69). Here we have fixed $\xi_{2nd}/L = 0.59238$. Fixing $Z_a/Z_p = 0.32037$ gives similar results. We see that the different estimates of y_t become consistent starting from $L_{min} \gtrsim 60$. As estimate we read off $y_t = 1.48875(45)$ corresponding to $\nu = 0.6717(2)$, which is consistent with the estimate given above, eq. (71), but less precise.

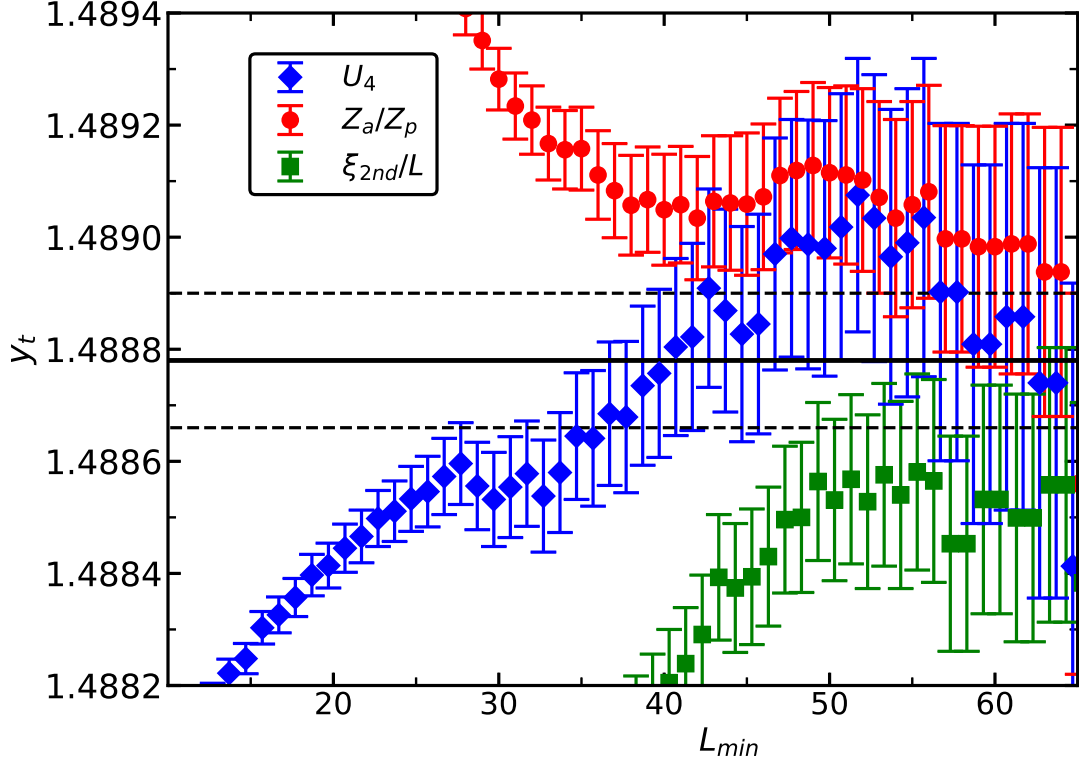


FIG. 11. Estimates of the RG-exponent y_t obtained from fitting the improved slopes of U_4 , Z_a/Z_p , and ξ_{2nd}/L at $\xi_{2nd}/L = 0.59238$ for $N = 8$ at $D = 1.05$ and 1.07 as a function of the minimal linear lattice size L_{min} that is taken into account. The ansatz (69) is used. To make the figure readable we shifted the values of L_{min} by -0.3 and 0.3 , for two of the slopes.

D. The energy density at the critical point

We analyzed the energy density, eq. (12), at our estimates of β_c for $D = 1.05$ and 1.07 . Here we do not consider a fixed value of Z_a/Z_p or ξ_{2nd}/L since this would generate contributions $\propto (\beta_f - \beta_c)$ from the analytic background of the energy density. Based on eq. (29), we fitted our data by using the ansätze

$$E = E_0 + aL^{-d+y_t} \quad , \quad (72)$$

$$E = E_0 + aL^{-d+y_t} (1 + cL^{-\epsilon_1}) \quad , \quad (73)$$

$$E = E_0 + aL^{-d+y_t} (1 + cL^{-\epsilon_1} + dL^{-\epsilon_2}) \quad , \quad (74)$$

where $\epsilon_1 = 2.02$ and $\epsilon_2 = y_t + \omega \approx 2.278$. In our joint fits for $D = 1.05$ and 1.07 , $E_0(1.05)$ and $E_0(1.07)$ are both free parameters of the fit. The same holds for $a(1.05)$ and $a(1.07)$. In

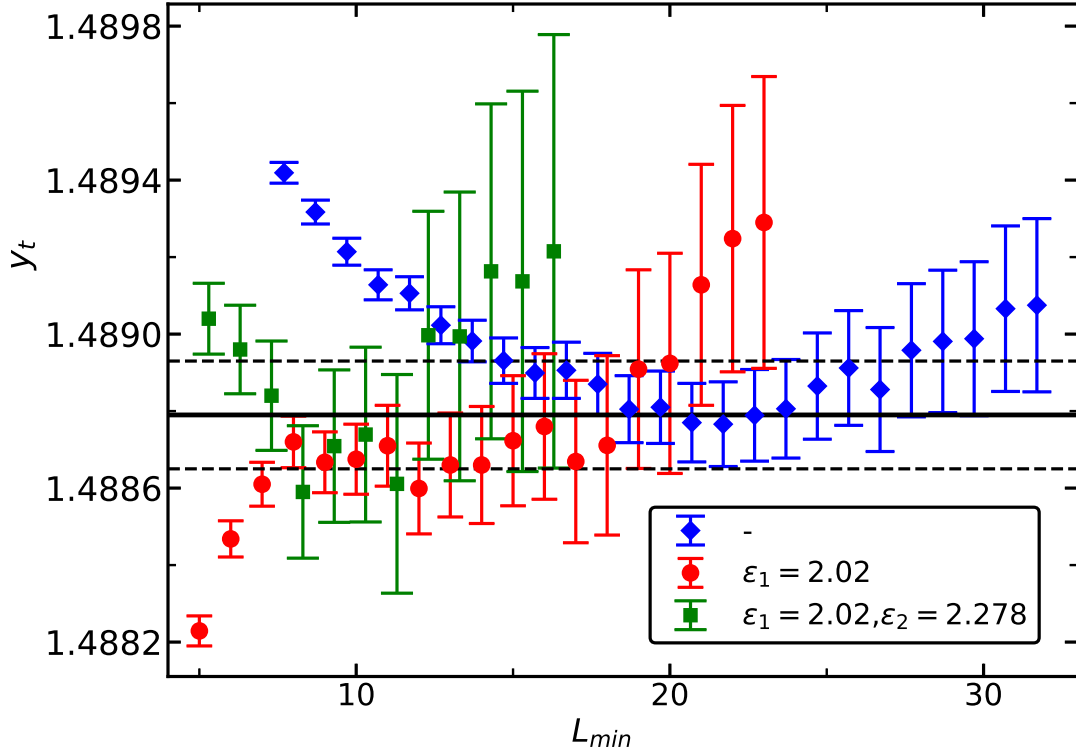


FIG. 12. Estimates for y_t obtained from analyzing the energy density. We fitted the data by using the ansätze (72,73,74). The corresponding correction exponents are given in the legend. L_{min} is the minimal linear lattice size that is included in the fits. Data for $N = 8$ at $D = 1.05$ and 1.07 are taken into account. For comparison we give the estimate of y_t obtained in the previous section by a straight solid line. The dashed lines give the error bar.

contrast, we set $c(1.05) = c(1.07)$ and $d(1.05) = d(1.07)$. In the case of the ansatz (72) we find $\chi^2/\text{d.o.f.} = 0.680$ for $L_{min} = 15$. In the case of the ansatz (73) we get $\chi^2/\text{d.o.f.} = 0.798$ for $L_{min} = 8$. For the ansatz (74) we get $\chi^2/\text{d.o.f.} = 0.931$ with $L_{min} = 5$. Our results for the RG-exponent y_t are shown in figure 12. For comparison we give the result obtained in the previous section by the solid horizontal line. The estimates of y_t obtained from the energy density are consistent with those obtained from the slopes of dimensionless ratios but a little less precise. Therefore we abstain from giving a final estimate of y_t based on the analysis of this section.

E. Exponent η from the behavior of the magnetic susceptibility χ

As observed in previous work [22], we find that the statistical error of χ is reduced, when computed at a fixed value of a phenomenological coupling compared with the error at a given value of $\beta \approx \beta_c$. Comparing U_4 , Z_a/Z_p and ξ_{2nd}/L we find that the reduction is clearly the largest for fixing $\xi_{2nd}/L = 0.59238$. For example for $D = 1.07$ and $L = 512$ we find a reduction of the statistical error by a factor of about 3.3 compared with χ at $\beta = 0.55888340$. This factor is slowly increasing with increasing lattice size.

Also here we analyzed the improved quantities

$$\bar{\chi}_{imp} = \bar{\chi} \bar{U}_4^p, \quad (75)$$

where both χ and U_4 are taken either at $Z_a/Z_p = 0.32037$ or $\xi_{2nd}/L = 0.59238$. We computed the exponent p in a similar way as in the previous section for S_R . Therefore we skip a detailed discussion and only report our results: $p = -0.97(2)$ and $-0.45(1)$ for $Z_a/Z_p = 0.32037$ and $\xi_{2nd}/L = 0.59238$, respectively.

We fitted our data with the ansätze

$$\bar{\chi}_{imp} = aL^{2-\eta}, \quad (76)$$

$$\bar{\chi}_{imp} = aL^{2-\eta} + b, \quad (77)$$

$$\bar{\chi}_{imp} = aL^{2-\eta}(1 + cL^{-\epsilon_2}) + b. \quad (78)$$

In the case of eq. (78), we fixed either $\epsilon_2 = 2.02$ or $\epsilon_2 = 4$.

Let us first discuss the analysis of the data for $Z_a/Z_p = 0.32037$ fixed. In figure 13 we plot our estimates of η obtained by using the ansätze (77) and (78). In figure 13, the analytic background is indicated by $\epsilon_1 = 2 - \eta$. In the case of ansatz (77) we find $\chi^2/\text{d.o.f.} = 0.899$ for $L_{min} = 16$. For the ansatz (78) $\chi^2/\text{d.o.f.}$ is less than one starting from $L_{min} = 11$ and 8 for $\epsilon_2 = 2.02$ and $\epsilon_2 = 4$, respectively. As our preliminary estimate we take $\eta = 0.03812(6)$. Fitting without correction term, eq. (76), $\chi^2/\text{d.o.f.} = 0.95$ is reached for $L_{min} = 40$. However the estimates of η are further increasing with increasing L_{min} . For $L_{min} = 96$ the estimates seem to level off. We get $\eta = 0.03813(15)$ for $L_{min} = 96$.

Next we turn to $\xi_{2nd}/L = 0.59238$. In figure 14 we plot our estimates of η obtained by using the ansätze (77) and (78). In the case of ansatz (77) we find $\chi^2/\text{d.o.f.} = 1.053$ for $L_{min} = 18$. For the ansatz (78) $\chi^2/\text{d.o.f.}$ is approximately one starting from $L_{min} = 18$ and

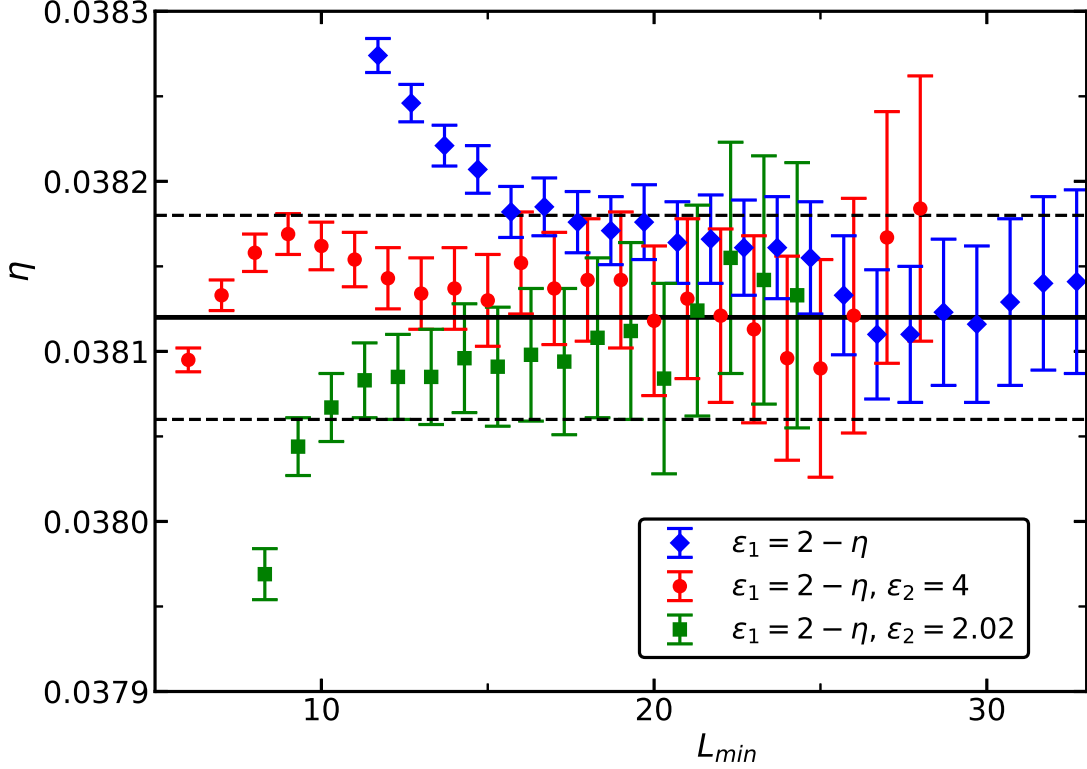


FIG. 13. Estimates of the critical exponent η obtained from fitting the improved magnetic susceptibility χ_{imp} at $Z_a/Z_p = 0.32037$ for $D = 1.05$ and 1.07 as a function of the minimal linear lattice size L_{min} that is taken into account. The ansätze (77,78) are used. To make the figure readable we shifted the values of L_{min} by -0.3 and 0.3 , for two of the fits.

14 for $\epsilon_2 = 2.02$ and $\epsilon_2 = 4$, respectively. As our preliminary estimate we take $\eta = 0.03808(3)$. Fitting without correction term, eq. (76), $\chi^2/\text{d.o.f.} = 1.336$ is reached for $L_{min} = 64$. For $L_{min} = 96$ we get $\eta = 0.03808(7)$.

We also analyzed the data for χ without improvement, eq. (75). We do not report the results in detail. They are consistent with those reported above.

As our final result we quote

$$\eta = 0.03810(8), \quad (79)$$

which is chosen such that the results obtained by using the ansätze (77,78) for fixing $Z_a/Z_p = 0.32037$ and $\xi_{2nd}/L = 0.59238$ are covered. As the last check we repeated the fits using the ansatz (77) for fixing $Z_a/Z_p = 0.32$ and 0.321 and $\xi_{2nd}/L = 0.592$ and $\xi_{2nd}/L = 0.593$. The variation of the results for η is well below the error quoted in eq. (79).

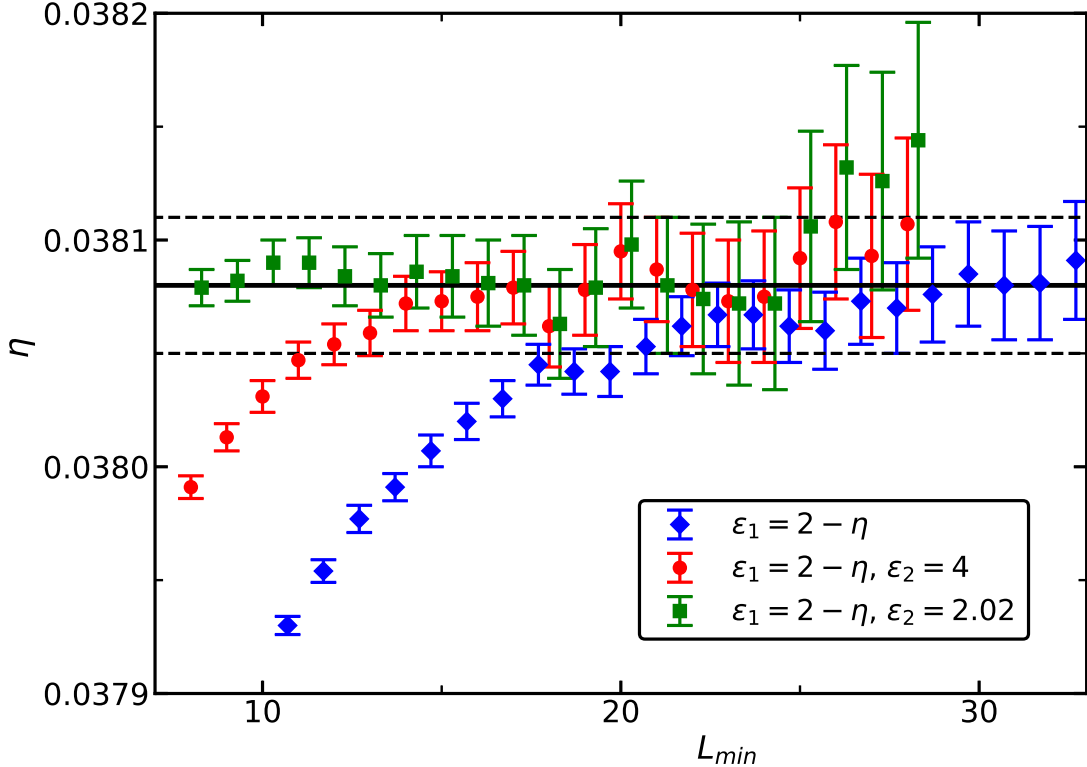


FIG. 14. Estimates of the critical exponent η obtained from fitting the improved magnetic susceptibility χ_{imp} at $\xi_{2nd}/L = 0.59238$ for $D = 1.05$ and 1.07 as a function of the minimal linear lattice size L_{min} that is taken into account. The ansätze (77,78) are used. To make the figure readable we shifted the values of L_{min} by -0.3 and 0.3 , for two of the fits.

VI. SUMMARY AND CONCLUSIONS

We have studied a generalized clock model on the simple cubic lattice by using a finite size scaling analysis. In the case of the N -state clock model, for $N \geq 5$, at the critical point, with increasing length scale, the Z_N symmetry is enhanced to $O(2)$; See for example [6]. In the generalized model, denoted by $(N + 1)$ -state clock model, $(0, 0)$ is added as allowed value of the spin. The parameter D , which controls the relative weight of $(0, 0)$, can be tuned such that the amplitude of leading corrections to scaling vanishes. We were aiming at accurate estimates of critical exponents for the three-dimensional XY universality class. Our motivation to study the $(N + 1)$ -state clock model is that the simulation requires less CPU-time and less memory than that of a model with $O(2)$ symmetry at the microscopic level.

In the main part of our study we considered $N = 8$. The RG-exponent related with a Z_8 symmetric perturbation of the $O(2)$ invariant fixed point takes the value $y_{N=8} = -5.278(9)$ [5]. Hence deviations from $O(2)$ symmetry vanish rapidly with increasing lattice size and can be ignored in the finite size analysis of the data. For $N = 8$ we find even for critical temperatures, which depend on the microscopic details of the model, only little differences compared with the $N \rightarrow \infty$ limit. For a detailed discussion see appendix B. In total we have spend the equivalent 50 years of CPU time on a single core of a Intel(R) Xeon(R) CPU E3-1225 v3 running at 3.20GHz.

Simulating the model for a large range of the parameter D we determined the exponent of the leading correction $\omega = 0.789(4)$ accurately. We located the tricritical point in the phase diagram. The corresponding $-0.87 < D_{tri} < -0.86$ is clearly smaller than $D^* = 1.058(13)$, where the amplitude of the leading correction vanishes. Focusing on the neighborhood of D^* we obtain $\eta = 0.03810(8)$ and $\nu = 0.67169(7)$, which are consistent with but more accurate than previous Monte Carlo results [12, 13]. The discrepancy with the experiments on the λ -transition of ${}^4\text{He}$ [8–10] is not dissolved. Note that the results of ref. [15], which appeared after we had submitted the first version of this paper, nicely agree with ours.

We determined the inverse of the critical temperature β_c for various values of D accurately. This is important information for coming studies. We plan compute two- and three-point functions at criticality on large lattices, similar to ref. [29], in order to get estimates for operator product expansion coefficients.

One might also study the low temperature phase of the improved $(N + 1)$ -state clock model. The consequences of the fact that a Z_N symmetric perturbation of the $O(2)$ symmetric fixed point is dangerously irrelevant in the low temperature phase are debated in the literature, as can be seen in [48] and references therein.

VII. ACKNOWLEDGEMENT

This work was supported by the DFG under the grant No HA 3150/5-1.

TABLE V. We give our numerical result for the inverse critical temperature β_c for $N = 8$ at the values of D not considered in section V A. Here we use $(Z_a/Z_p)^* = 0.32037(6)$. The number given in [] is the error due to the uncertainty of $(Z_a/Z_p)^*$.

D	β_c
∞	0.45416467(10)[7]
1.24	0.54365020(30)[10]
0.9	0.57645235(30)[11]
0.45	0.63625739(10)[8]
0.0	0.7191494(3)[1]
-0.5	0.8423571(7)[1]
-0.7	0.9008977(10)[1]

Appendix A: The inverse critical temperature for $N = 8$

Here we compute β_c for those values of D that are not consider in section V A. To this end we analyze the behavior of Z_a/Z_p and ξ_{2nd}/L . We fit our data with the ansätze

$$R(\beta_c) = R^* + bL^{-\epsilon} , \quad (\text{A1})$$

$$R(\beta_c) = R^* + bL^{-\epsilon} + cL^{-2\epsilon} , \quad (\text{A2})$$

$$R(\beta_c) = R^* + bL^{-\epsilon} + cL^{-2\epsilon} + dL^{-3\epsilon} \quad (\text{A3})$$

using $\epsilon = 0.789$. As in section V A, we compute $R(\beta)$ by using its Taylor expansion around β_s up to the third order. The free parameters of the fits are β_c , b , c , and d . R^* is fixed by the numerical results obtained in section V A. Our results for $Z_a/Z_p = 0.32037$ are summarized in table V. The results obtained for $\xi_{2nd}/L = 0.59238$ are compatible.

Appendix B: The N -dependence of the inverse critical temperature and D^*

1. The Caley tree

In order to get a first idea, we have computed numerically β_c for the model put on a Caley tree with the coordination number $z = 6$. The phase transition is of mean-field

TABLE VI. We give our numerical result for the inverse critical temperature $\beta_{c,Caley}$ for the Caley tree with coordination number $z = 6$.

$N \setminus D$	∞	1	0
5	0.4081307306	0.5224090169	0.6890295689
6	0.4082712294	0.5227444788	0.6898803344
7	0.4082770202	0.5227621638	0.6899394147
8	0.4082772183	0.5227629375	0.6899428166
9	0.4082772241	0.5227629665	0.6899429844
10	0.4082772243	0.5227629675	0.6899429916
11	0.4082772243	0.5227629675	0.6899429919
12	0.4082772243	0.5227629675	0.6899429919

type. However β_c for the Caley tree should be a better approximation of β_c for the three-dimensional model than simple mean-field.

For given values of D and $\beta > \beta_c$ we computed the magnetization. Estimates of the inverse critical temperature are obtained by solving

$$m = c(\beta - \beta_c)^{1/2} \quad (\text{B1})$$

for two different values of β with respect to c and β_c . Iteratively we diminish $\beta - \beta_c$ until corrections to eq. (B1) can be ignored. This way we obtain the critical temperature up to about 10 accurate digits.

We computed β_c for $D = \infty, 1.0$ and 0.0 and $N = 5, 6, \dots, 12$. Our results are given in table VI. We find that, at the level of our precision, the results are identical starting from $N = 10$ for $D = \infty$ and $D = 1$. For $D = 0$ this holds starting from $N = 11$. Deviations from the limit $N \rightarrow \infty$ seem to increase with decreasing D . The approach $N \rightarrow \infty$ is compatible with an exponential decay with a large, D dependent, decay rate.

2. N -dependence of β_c : three-dimensional model

We performed simulations for $N \neq 8$ for a small number of lattice sizes. We determined $\beta_{f,Z_a/Z_p=0.32037}$, where $Z_a/Z_p = 0.32037$ and $\beta_{f,\xi_{2nd}/L=0.59238}$, where $\xi_{2nd}/L = 0.59238$. Since

the difference of β_c for different values of N is essentially related to the microscopic details of the model at small scales, we expect that differences or ratios of β_f obtained for moderate lattice sizes are good approximations of the differences or ratios of β_c . Note that Z_a/Z_p is only defined for even values of N . We study the ratio

$$r(L) = \frac{\beta_{f,N=8}(L)}{\beta_{f,N}(L)}. \quad (\text{B2})$$

As discussed in section III, there is an N dependence of all scaling fields. In particular there should be a, even though small, dependence of the scaling field related to the leading correction to scaling. Therefore we expect that

$$r(L) = \frac{\beta_{c,N=8}}{\beta_{c,N}} + cL^{-\epsilon} + \dots \quad (\text{B3})$$

where $\epsilon = 1/\nu + \omega$ is the exponent related with the leading correction. We performed simulations for $D = \infty$, 1.07, and $D = 1.02$. Let us first discuss our results for $D = \infty$. For $N = 6$ we simulated the linear lattice sizes $L = 32, 36$, and 40. The ratios, eq. (B2), for these three lattice sizes are consistent within their error bars. The average is given in table VII. For $N = 7$ we simulated the lattice sizes $L = 36$ and 40. For $N = 10$ we simulated the lattice sizes $L = 32, 40$ and 48. Also for these two values of N , the averages are given in table VII. In addition we make use of the estimates $1/\beta_{c,N=5} = 2.20502(1)$ and $1/\beta_{c,N=6} = 2.20201(1)$ reported in [48]. Note that for $N = 6$ the result of [48] is fully consistent with ours. Similar to the Caley tree approximation, we see a rapid convergence of $\beta_{c,N}$ with $N \rightarrow \infty$. Already for $N = 8$ and 10, we can not find a difference at our level of accuracy. Extrapolating the ratios for smaller values of N we get $\beta_{c,N=8}/\beta_{c,9} \approx 0.99999985$. At our level of precision, the same ratio holds for all $N \geq 9$. Using this estimate, we arrive at $\beta_{c,XY} = 0.45416474(10)$ [7]. In table VIII we summarize estimates of $\beta_{c,XY}$ given in the literature.

Next let us discuss the results for $D = 1.07$. Here we simulated the linear lattice sizes $L = 64$ for $N = 6$, $L = 32, 40, 48$, and 64 for $N = 7$ and $L = 48$ and 64 for $N = 12$. The averages of the ratios of β_f are reported in table VII. Similar to $D = \infty$ we see a rapid convergence of $\beta_{c,N}$, which is however slightly slower than it is the case for $D = \infty$. In particular our estimate for $\beta_{c,N=8}/\beta_{c,N=12}$ differs from 1 by about 3.6 times the error bar. Extrapolating the results for $N < 8$ we arrive at $\beta_{c,N=8}/\beta_{c,N>8} \approx 0.9999995$.

Finally for $D = 1.02$ we have simulated $L = 4, 5, \dots, 14, 16, 18, 20$, and 64 for $N = 6$. These simulations were performed at an early stage of the study, mainly to determine the

TABLE VII. We give our numerical estimates for the ratio $r = \beta_{c,N=8}/\beta_{c,N}$ obtained from $\beta_{f,Z_a/Z_p=0.32037}$ and $\beta_{f,\xi_{2nd}/L=0.59238}$. In addition results based on ref. [48] are reported.

D	N	$Z_a/Z_p = 0.32037$	$\xi_{2nd}/L = 0.59238$	ref. [48]
∞	5	-	-	1.001442(5)
∞	6	1.00007847(22)	1.00007837(20)	1.000075(5)
∞	7	-	1.00000362(21)	-
∞	10	1.00000015(21)	0.99999984(20)	-
1.07	6	1.00017147(32)	1.00017141(29)	-
1.07	7	-	1.00000946(15)	-
1.07	12	0.99999938(16)	0.99999947(16)	-
1.02	6	1.0001772(3)	1.0001769(3)	-

correction exponent y_6 . Here we see a dependence of the ratio r , eq. (B2), on the lattice size L . First we analyzed the results obtained for $\beta_{f,Z_a/Z_p=0.32037}$. We fitted our data with the ansatz

$$r(L) = a + cL^{-\epsilon} , \quad (\text{B4})$$

using the numerical value $\epsilon = 1/\nu + \omega = 2.27779$. Including data with $L \geq 8$ we get $a = 1.0001772(3)$, $c = 0.00155(12)$ and $\chi^2/\text{d.o.f.} = 0.70$. The analysis of the data for $\beta_{f,\xi_{2nd}/L=0.59238}$ gives very similar results. Our final estimates are given in table VII.

3. N -dependence of D^*

As discussed in section III, the value of D^* depends on N . To get a numerical estimate, we analyze the Binder cumulant \bar{U}_4 at either $Z_a/Z_p = 0.32037$ or $\xi_{2nd}/L = 0.59238$ at values of D close to D^* .

First we estimate the slope of the correction amplitude close to D^* for $N = 8$ by fitting the data with the ansatz

$$\bar{U}_4(N = 8, D = 1.07) - \bar{U}_4(N = 8, D = 1.02) = b_d L^{-\omega} , \quad (\text{B5})$$

TABLE VIII. We summarize results from the literature for the inverse critical temperature of the XY model on the simple cubic lattice.

ref.	year	β_c
[46]	2005	0.4541655(10)
[12]	2006	0.4541652(5)[6]
[47]	2012	0.45416313(20)
[47]	2012	0.45416742(12)
[38]	2014	0.4541664(12)
[13]	2019	0.45416466(10)
this work	2019	0.45416474(10)[7]

where we have fixed $\omega = 0.789$, or

$$\bar{U}_4(N = 8, D = 1.07) - \bar{U}_4(N = 8, D = 1.02) = b_d L^{-\omega} + c_d L^{-2}. \quad (\text{B6})$$

In the following we assume that the dependence of

$$\left. \frac{db}{dD} \right|_{D=D^*} \approx \frac{b_d}{0.05} \quad (\text{B7})$$

on N can be ignored. We get $b_d = -0.00616(10)$ for fixing $Z_a/Z_p = 0.32037$ and $b_d = -0.00705(16)$ for fixing $\xi_{2nd}/L = 0.59238$.

In the second step, we analyze how \bar{U}_4 changes with N at a fixed value of D . To this end we define

$$\Delta_U(N_1, N_2, D) = \bar{U}_4(N_1, D) - \bar{U}_4(N_2, D), \quad (\text{B8})$$

where here $N_2 = 8$. We fitted our data with the ansätze

$$\Delta_U(N_1, N_2, D) = \Delta_b(N_1, N_2, D) L^{-\omega}, \quad (\text{B9})$$

where we have fixed $\omega = 0.789$ and

$$\Delta_U(N_1, N_2, D) = \Delta_b(N_1, N_2, D) L^{-\omega} + \Delta_c(N_1, N_2, D) L^{-\epsilon}, \quad (\text{B10})$$

where we fixed $\epsilon = 2$. In the case of $N_1 = 6$ we used in addition $\epsilon = 2.4$. The shift in D^* is given by

$$D^*(N_1) - D^*(8) \approx -\Delta_b(N_1, 8, D) \frac{0.05}{b_d}. \quad (\text{B11})$$

For the purpose of this section, we have simulated the linear lattice size $L = 4, 5, 6, \dots$, and 16 for $N = 10$ at $D = 1.07$ with a statistics similar to that for $N = 8$. It turns out that $\Delta_U(10, 8, 1.07)$ is compatible with zero for most of the lattice sizes. Fitting the data for $L \geq 8$ with the ansatz (B9) we get $\Delta_b(10, 8, 1.07) = -0.000004(10)$ and $-0.000012(10)$ for fixing $Z_a/Z_p = 0.32037$ and $\xi_{2nd}/L = 0.59238$, respectively. Fitting with the ansatz (B10), the estimates stay compatible with zero, but with a larger error bar. Taking also these results into account we conclude that $|D^*(10) - D^*(8)| \lesssim 0.0005$.

Next we have analyzed our data for $N = 6$ and $D = 1.02$. Taking into account the results of the fits using different ansätze, we arrive at $\Delta_b(6, 8, 1.02) = 0.00163(6)$ for fixing $Z_a/Z_p = 0.32037$ and $\Delta_b(6, 8, 1.02) = 0.00198(13)$ for fixing $\xi_{2nd}/L = 0.59238$. Plugging in the numbers into eq. (B11) we arrive at $D^*(6) - D^*(8) = 0.0132(5)$ and $0.0140(10)$, for fixing $Z_a/Z_p = 0.32037$ or $\xi_{2nd}/L = 0.59238$, respectively. As our final result we take

$$D^*(6) - D^*(8) = 0.0136(14) \tag{B12}$$

covering both the results for fixing $Z_a/Z_p = 0.32037$ and for fixing $\xi_{2nd}/L = 0.59238$.

Assuming that $D^*(N)$ converges rapidly to $D^*(\infty)$, we conclude that $|D^*(N) - D^*(8)|$ for $N > 8$ is much smaller than the error of $D^*(8)$, eq. (63). It seems plausible that $D^*(7) - D^*(8)$ is smaller than $D^*(6) - D^*(8)$ computed above. Likely $|D^*(5) - D^*(8)|$ is considerably larger than the error of $D^*(8)$ and an effort beyond that of this section is required to obtain an accurate estimate of $D^*(5)$.

4. N -dependence of the magnetic susceptibility and the slope of dimensionless quantities

Finally we have studied the dependence of quantities that we used to compute the critical exponents ν and η on N . In particular we consider the magnetic susceptibility and the slopes of dimensionless quantities at either $Z_a/Z_p = 0.32037$ or $\xi_{2nd}/L = 0.59238$. Let us discuss the results obtained for the susceptibility. Those for the slopes of dimensionless quantities are qualitatively the same.

We computed the ratio

$$R_\chi(6, 8) = \frac{\chi(N=6)}{\chi(N=8)} \tag{B13}$$

for either $Z_a/Z_p = 0.32037$ or $\xi_{2nd}/L = 0.59238$ fixed at $D = 1.02$. Following the discussion of section III, this ratio should behave as

$$R_\chi(6, 8) = a (1 + bL^{-\omega} + \dots) , \quad (\text{B14})$$

where all possible types of corrections should appear, and not only those related to the breaking of the $O(2)$ symmetry. We have fitted our data by using a single correction term. In the case of $Z_a/Z_p = 0.32037$ we get the following results:

Using the correction exponent $\epsilon = 0.789$ and $L_{min} = 6$ we get $a = 1.000187(14)$, $b = 0.00126(8)$ and $\chi^2/\text{d.o.f.} = 0.36$. Using instead $\epsilon = 2$ and $L_{min} = 8$ we get $a = 1.000295(9)$, $b = 0.0091(10)$ and $\chi^2/\text{d.o.f.} = 0.56$.

For $\xi_{2nd}/L = 0.59238$ fixed we get: Using the correction exponent $\epsilon = 0.789$ and $L_{min} = 8$ we get $a = 1.000222(15)$, $b = -0.00010(11)$ and $\chi^2/\text{d.o.f.} = 0.64$. Using instead $\epsilon = 2$ and $L_{min} = 4$ we get $a = 1.000219(4)$, $b = -0.00143(13)$ and $\chi^2/\text{d.o.f.} = 0.59$.

We conclude that the ratio (B13) consists of an overall constant that is close to one and corrections with a small amplitude. Since these corrections come with a very small amplitude, it is impossible to assign them clearly to the correction exponents that are theoretically expected.

In the case of $N = 8$ and $N = 10$ at $D = 1.07$ the data barely differ. For example for χ at $\xi_{2nd}/L = 0.59238$ we get for $L = 4$ the estimates $17.01708(4)$ and $17.01707(5)$, respectively. Therefore we abstain from any further analysis.

Appendix C: The correction exponent $y_{N=6}$

We define

$$X_N = \langle \max_j \vec{m} \vec{r}_j \rangle , \quad (\text{C1})$$

$$Y_N = \langle \max_j \vec{m} \vec{p}_j \rangle , \quad (\text{C2})$$

where

$$\vec{r}_j = (\cos(2\pi j/N), \sin(2\pi j/N)) , \quad (\text{C3})$$

$$\vec{p}_j = (\cos(2\pi[j + 1/2]/N), \sin(2\pi[j + 1/2]/N)) , \quad (\text{C4})$$

where $j \in \{0, \dots, N - 1\}$ and

$$(m^{(0)}, m^{(1)}) = \vec{m} = \sum_x \vec{s}_x \quad (\text{C5})$$

is the magnetization. Now we consider the quantity

$$q_N = \frac{X_N - Y_N}{X_N + Y_N} \quad (\text{C6})$$

as a measure of the deviation from $O(2)$ invariance. We performed simulations for $N = 6$ and $D = 1.02$ close to our final estimate of $D^*(6) = 1.058(13) + 0.0136(14)$. We simulated the lattice sizes $L = 4, 5, \dots, 16, 18, 20$, and 64 , as discussed already above. The quantities X_N and Y_N are taken at $Z_a/Z_p = 0.32037$. Note that q_N for $L = 64$ is equal to zero within error bars. Therefore we did not include $L = 64$ in our analysis. We fitted our numerical results with the ansätze

$$q_N = cL^{y_{N=6}} \quad (\text{C7})$$

and

$$q_N = cL^{y_{N=6}} \times (1 + bL^{-2}) . \quad (\text{C8})$$

We find $y_{N=6} = -2.42(2)$ and $\chi^2/\text{d.o.f.} = 0.53$ with $L_{min} = 8$ using the first ansatz and $y_{N=6} = -2.46(3)$ and $\chi^2/\text{d.o.f.} = 0.59$ with $L_{min} = 6$ using the second ansatz. As our final estimate we take $y_{N=6} = -2.43(6)$, where the error estimate includes the results of both fits.

This value has to be compared with $y_{N=6} = -2.55(6)$ and $-2.509(7)$ given in refs. [48] and [5], respectively.

Note that for $N > 6$ it is virtually impossible to get a reliable estimate of y_N using the method used here, since the relative error of q_N is rapidly increasing with increasing L .

At a late stage of the project we have implemented the quantity

$$\phi_N = \langle \cos(N\Theta) \rangle , \quad (\text{C9})$$

where $\Theta = \arccos(m^{(0)}/|\vec{m}|)$, which is used in ref. [48]; See eq. (3) of ref. [48]. We simulated the linear lattice sizes $L = 4, 6, 8$, and 12 , measuring both ϕ_N and q_N . We find that the relative error is slightly smaller for q_N , the two quantities are highly correlated, and their ratio ϕ_N/q_N is within the statistical error the same for the lattice sizes $L = 6, 8$, and 12 . For $L = 4$ it deviates by little. Hence for our purpose the two quantities are equivalent.

[1] K. G. Wilson and J. Kogut, *The renormalization group and the ϵ -expansion*, Phys. Rep. C **12**, 75 (1974).

- [2] M. E. Fisher, *The renormalization group in the theory of critical behavior*, Rev. Mod. Phys. **46**, 597 (1974).
- [3] M. E. Fisher, *Renormalization group theory: Its basis and formulation in statistical physics*, Rev. Mod. Phys. **70**, 653 (1998).
- [4] A. Pelissetto and E. Vicari, *Critical Phenomena and Renormalization-Group Theory*, [cond-mat/0012164], Phys. Rept. **368**, 549 (2002).
- [5] D. Banerjee, S. Chandrasekharan, and D. Orlando, *Conformal dimensions via large charge expansion*, [arXiv:1707.00711], Phys. Rev. Lett. **120**, 061603 (2018).
- [6] J. Hove and A. Sudbø, *Criticality versus q in the $(2+1)$ -dimensional Z_q clock model*, [arXiv:cond-mat/0301499], Phys. Rev. E **68**, 046107 (2003).
- [7] Jie Lou, Anders W. Sandvik, and Leon Balents, *Emergence of $U(1)$ Symmetry in the 3D XY Model with Z_q Anisotropy*, [arXiv:0704.1472], Phys. Rev. Lett. **99**, 207203 (2007).
- [8] J. A. Lipa, D. R. Swanson, J. A. Nissen, T. C. P. Chui, and U. E. Israelsson, *Heat Capacity and Thermal Relaxation of Bulk Helium very near the Lambda Point*, Phys. Rev. Lett. **76**, 944 (1996).
- [9] J. A. Lipa, D. R. Swanson, J. A. Nissen, Z. K. Geng, P. R. Williamson, D. A. Stricker, T. C. P. Chui, U. E. Israelsson, and M. Larson, *Specific Heat of Helium Confined to a 57- μm Planar Geometry*, Phys. Rev. Lett. **84**, 4894 (2000).
- [10] J. A. Lipa, J. A. Nissen, D. A. Stricker, D. R. Swanson and T. C. P. Chui, *Specific heat of liquid helium in zero gravity very near the λ -point*, [arXiv:cond-mat/0310163], Phys. Rev. B **68**, 174518 (2003).
- [11] R. Guida and J. Zinn-Justin, *Critical exponents of the N vector model*, [arXiv:cond-mat/9803240], J. Phys. A **31**, 8103 (1998).
- [12] M. Campostrini, M. Hasenbusch, A. Pelissetto, and E. Vicari, *The critical exponents of the superfluid transition in He4*, [cond-mat/0605083], published as *Theoretical estimates of the critical exponents of the superfluid transition in He4 by lattice methods*, Phys. Rev. B **74** (2006) 144506.
- [13] W. Xu, Y. Sun, J.-P. Lv, and Y. Deng, *High-precision Monte Carlo study of several models in the three-dimensional $U(1)$ universality class*, [arXiv:1908.10990], Phys. Rev. B **100**, 064525 (2019).
- [14] F. Kos, D. Poland, D. Simmons-Duffin, and A. Vichi, *Precision Islands in the Ising and $O(N)$*

- Models [arXiv:1603.04436], JHEP 08 (2016) 036.
- [15] S. M. Chester, W. Landry, J. Liu, D. Poland, D. Simmons-Duffin, N. Su, and A. Vichi, *Carving out OPE space and precise $O(2)$ model critical exponents*, [arXiv:1912.03324].
- [16] M. Campostrini, M. Hasenbusch, A. Pelissetto, P. Rossi, and E. Vicari, *Critical behavior of the three-dimensional XY universality class*, [cond-mat/0010360], Phys. Rev. B **63** (2001) 214503.
- [17] D. Simmons-Duffin, *The Lightcone Bootstrap and the Spectrum of the 3d Ising CFT*, [arXiv:1612.08471], JHEP 03 (2017) 086.
- [18] J. H. Chen, M. E. Fisher and B. G. Nickel, *Unbiased Estimation of Corrections to Scaling by Partial Differential Approximants*, Phys. Rev. Lett. **48**, 630 (1982).
- [19] M. E. Fisher and J. H. Chen, *The validity of hyperscaling in three dimensions for scalar spin systems*, J. Physique (Paris) **46**, 1645 (1985).
- [20] H. W. J. Blöte, E. Luijten and J. R. Heringa, *Ising universality in three dimensions: a Monte Carlo study*, [arXiv:cond-mat/9509016], J. Phys. A: Math. Gen. **28**, 6289 (1995).
- [21] H. G. Ballesteros, L. A. Fernández, V. Martín-Mayor, and A. Muñoz Sudupe, *Finite Size Scaling and perfect actions: the three dimensional Ising model*, [arXiv:hep-lat/9805022], Phys. Lett. B **441**, 330 (1998).
- [22] M. Hasenbusch, K. Pinn, and S. Vinti, *Critical Exponents of the 3D Ising Universality Class From Finite Size Scaling With Standard and Improved Actions*, [arXiv:hep-lat/9806012], Phys. Rev. B **59**, 11471 (1999).
- [23] M. N. Barber, *Finite-size Scaling in Phase Transitions and Critical Phenomena, Vol. 8*, eds. C. Domb and J. L. Lebowitz, (Academic Press, 1983)
- [24] M. Hasenbusch, *A Monte Carlo study of leading order scaling corrections of ϕ^4 theory on a three dimensional lattice*, [hep-lat/9902026], J. Phys. A **32**, 4851 (1999).
- [25] M. Hasenbusch and T. Török, *High precision Monte Carlo study of the 3D XY-universality class* [arXiv:cond-mat/9904408], J. Phys. A **32**, 6361 (1999).
- [26] M. Hasenbusch, F. Parisen Toldin, A. Pelissetto, and E. Vicari, *Universality class of 3D site-diluted and bond-diluted Ising systems*, [arXiv:cond-mat/0611707], J. Stat. Mech.: Theory Exp. **2007**, P02016.
- [27] M. Hasenbusch, *A Finite Size Scaling Study of Lattice Models in the 3D Ising Universality Class*, [arXiv:1004.4486], Phys. Rev. B **82**, 174433 (2010).

- [28] K. Binder, *Finite Size Scaling Analysis of Ising Model Block Distribution Functions*, Z. Phys. B: Condens. Matter **43**, 119 (1981).
- [29] M. Hasenbusch, *Two- and three-point functions at criticality: Monte Carlo simulations of the improved three-dimensional Blume-Capel model*, [arXiv:1711.10946], Phys. Rev. E **97** (2018) 012119.
- [30] A. Maciolek, M. Krech, and S. Dietrich, *Phase diagram of a model for ^3He - ^4He mixtures in three dimensions*, Phys. Rev. E **69**, 036117 (2004).
- [31] M. Campostrini, A. Pelissetto, P. Rossi, and E. Vicari, *Two-point correlation function of three-dimensional $O(N)$ models: The critical limit and anisotropy*, [arXiv:cond-mat/9705086], Phys. Rev. E **57**, 184 (1998).
- [32] U. Wolff, *Collective Monte Carlo Updating for Spin Systems*, Phys. Rev. Lett. **62**, 361 (1989).
- [33] M. Campostrini, A. Pelissetto, P. Rossi, and E. Vicari, *25th order high temperature expansion results for three-dimensional Ising like systems on the simple cubic lattice*, [arXiv:cond-mat/0201180], Phys. Rev. E **65**, 066127 (2002).
- [34] K. E. Newman and E. K. Riedel, *Critical exponents by the scaling-field method: The isotropic N -vector model in three dimensions*, Phys. Rev. B **30**, 6615 (1984).
- [35] D. F. Litim and L. Vergara, *Subleading critical exponents from the renormalisation group*, [arXiv:hep-th/0310101], Phys. Lett. B **581**, 263 (2004).
- [36] A. Jüttner, D.F. Litim, and E. Marchais, *Global WilsonFisher fixed points*, [arXiv:1701.05168], Nucl. Phys. B **921**, 769 (2017).
- [37] M. Weigel, *Simulating spin models on GPU*, Comput. Phys. Commun. **182**, 1833 (2011).
- [38] Y. Komura and Y. Okabe, *CUDA programs for GPU computing of Swendsen-Wang multi-cluster spin flip algorithm: 2D and 3D Ising, Potts, and XY models*, [arXiv:1403.7560], Comput. Phys. Commun. **185**, 1038 (2014); *ibid.*, *Improved CUDA programs for GPU computing of Swendsen-Wang multi-cluster spin flip algorithm: 2D and 3D Ising, Potts, and XY models*, **200**, 400 (2016).
- [39] M. Saito and M. Matsumoto, “SIMD-oriented Fast Mersenne Twister: a 128-bit Pseudorandom Number Generator”, in *Monte Carlo and Quasi-Monte Carlo Methods 2006*, edited by A. Keller, S. Heinrich, H. Niederreiter, (Springer, 2008); M. Saito, Masters thesis, Math. Dept., Graduate School of science, Hiroshima University, 2007. The source code of the program is provided at <http://www.math.sci.hiroshima-u.ac.jp/~m-mat/MT/SFMT/index.html>

- [40] J. D. Hunter, "Matplotlib: A 2D Graphics Environment, Computing in Science & Engineering **9**, 90 (2007).
- [41] T. E. Oliphant, *Python for Scientific Computing*, Computing in Science & Engineering **9**, 10 (2007); E. Jones, E. Oliphant, P. Peterson, et al., *SciPy: Open Source Scientific Tools for Python*, 2001-, <http://www.scipy.org/>, P. Virtanen, R. Gommers, T. E. Oliphant et al., *SciPy 1.0—Fundamental Algorithms for Scientific Computing in Python*, [arXiv:1907.10121].
- [42] K. Levenberg, *A method for the solution of certain non-linear problems in least squares*, Quart. Appl. Math. **2**, 164 (1944).
- [43] D. Marquardt, *An Algorithm for Least-Squares Estimation of Nonlinear Parameters*, SIAM J. Appl. Math. **11**, 431, (1963).
- [44] J. J. Moré, *The Levenberg-Marquardt algorithm: Implementation and theory*, in G. A. Watson (ed.): Numerical Analysis. Dundee 1977, Lecture Notes Math. **630**, 105 (1978).
- [45] J. J. Moré, B. S. Garbow, and K. E. Hillstom, *User Guide for MINPACK-1*, Argonne National Laboratory Report ANL-80-74, Argonne, Ill., (1980); J. J. Moré, D. C. Sorensen, K. E. Hillstom, and B. S. Garbow, *The MINPACK Project*, in Sources and Development of Mathematical Software, W. J. Cowell, ed., Prentice-Hall, 88 (1984).
- [46] Y.J. Deng, H.W.J. Blöte, M.P. Nightingale, *Surface and bulk transitions in three-dimensional $O(n)$ models*, [arXiv:cond-mat/0504173], Phys. Rev. E **72**, 016128 (2005).
- [47] T.-Y. Lan, Y.-D. Hsieh, and Y.-J. Kao, *High-precision Monte Carlo study of the three-dimensional XY model on GPU*, [arXiv:1211.0780].
- [48] H. Shao, W. Guo, and A. W. Sandvik, *Monte Carlo Renormalization Flows in the Space of Relevant and Irrelevant Operators: Application to Three-Dimensional Clock Models*, [arXiv:1905.13640].